Med Biol Eng Comput (2010) 48:977–998
DOI 10.1007/s11517-010-0649-3

SPECIAL ISSUE - REVIEW

Magnetic biosensor technologies for medical applications: a review

J. Llandro · J. J. Palfreyman · A. Ionescu · C. H. W. Barnes

Received: 15 January 2010 / Accepted: 2 June 2010 / Published online: 24 June 2010

Abstract In this review we discuss conventional methods of performing biological assays and molecular identification and highlight their advantages and limitations. An alternative approach based on magnetic nanotechnology is then presented. Firstly, magnetic carriers are introduced and their biocompatibility and functionalisation discussed, with spotlights on functionalisation via self assembled monolayers and on methods of reducing nonspecific binding. In addition an introduction is provided to the basic physical concepts behind the various types of sensors used to detect magnetic labels. Finally, progress in the field of magnetic biosensors and the outlook for the future are discussed.

Keywords Magnetic biosensors · Magnetic nanoparticles · Functionalisation · Biomedicine

Abbreviations

AFM	Atomic force microscope
AMR	Anisotropic magnetoresistance
CIP	Current in-plane
CPP	Current perpendicular-to-plane
dNTPs	Deoxynucleotide triphosphates
FM	Ferromagnet
FET	Field effect transistor
FRET	Fluorescence resonance energy transfer
GMR	Giant magnetoresistance
MR	Magnetoresistance
MRI	Magnetic resonance imaging
μTAS	Microscopic total analysis systems
MTJ	Magnetic tunnel junction
NHS	N-Hydroxysuccinimide
PCR	Polymerase chain reaction
PEG	Poly(ethylene) glycol
PSV	Pseudo-spin-valve
QDs	Quantum dots
RT	Room temperature
SAM	Self assembled monolayer
SEM	Scanning electron microscopy
SQUID	Super-conducting quantum interference device
SV	Spin-valve
TMR	Tunnelling magnetoresistance

J. Llandro (✉) · J. J. Palfreyman · A. Ionescu · C. H. W. Barnes
Cavendish Laboratory, J.J. Thomson Avenue, Cambridge CB3 0HE, UK
e-mail: jl286@cam.ac.uk

A. Ionescu
e-mail: ai222@cam.ac.uk

1 Introduction

The last decade has seen an enormous surge of work being carried out on biomagnetism and magnetic biosensors based on molecular recognition processes. Recent reviews focussing on applications of magnetic nanoparticles in biomedicine [129], their synthesis [142] and functionalisation [16] and their detection by magnetic sensors [109] underpin these efforts. New avenues of research and clinical methods have been successfully established, such as magnetic actuation, hyperthermia treatment, targeted drug delivery and the use of magnetic particles as MRI contrast agents, but also well established sequencing methods in genetics or bioassays based on fluorescent detection have been challenged. Without any doubt advances have been made in modern bioassays, nevertheless there is still space for improvement related to the speed of detection, costs

and specificity. It is exactly here where magnetic sensor based bioassays propose to make a difference.

2 Bioassay technologies

2.1 Microarrays

DNA microarrays (also known as gene chips or DNA chips) [149] are most commonly used to detect the presence, activity or variation of thousands of genes simultaneously, using only picolitres of reagents. Such microarrays identify hybridisation of a particular fluorescently or radioisotopically labelled probe (a short stretch of single-stranded DNA) to the analyte sequence by observation of a spatially resolved optical signal.

There are two variants of DNA microarray technology, depending on the size of the probe molecule, as measured in pairs of DNA bases making up the double helix, or base pairs (bp). For 'traditional' DNA microarrays, probes are presynthesised complementary DNA (cDNA) sequences around 500–5000 bp long, and are immobilised to a glass or plastic plate either covalently or by electrostatic attraction between the plate and the phosphate backbone of the DNA. The cDNA probes are added to predetermined sites on the microarray plate to define features about 100 μm across by contact printing or spotting (complete presynthesised probes are deposited onto the sites by pins or piezoelectric nozzles in a robot). For DNA oligonucleotides (20–200 bp), the microarray plate is functionalised with chemical linkers which covalently bond the short DNA sections to the plate via a silane or an aliphatic amine (NH_2) group. In this case, the features can be created either by conventional synthesis followed by immobilisation, or alternatively by in situ probe synthesis. Primers are added to all sites and then the array is washed with a solution containing one kind of nucleotide, which is added to the primers by using light to remove a blocking chemical group (deprotection) on the end of the last base. Successive repetitions of the process assemble the complete probes, which for photodeprotection are around 25 bp long. Selective illumination of the features is accomplished by photolithographic masks [45] or in maskless fashion by micromirror arrays [156]. State of the art microarrays of this type, known as DNA chips,[1] contain around 500,000 features for spotted arrays, 800,000 features for masklessly fabricated arrays and 1.6 million features or more for masked arrays (Fig. 1). Recently, direct inkjet printing has been used to alternately add nucleotides and a chemical deprotection agent to the sites to build up the probes base by base to a length of about 60 bp [69]. However, using a phosphoramidite–tetrazole (P–T) chemistry [30], researchers at Agilent Technologies (Inc.) have been able to synthesise 150–175 bp oligonucleotides in situ with a stepwise yield of 99.5% and error rate of 1 bp in 250–300 [133]. A five-nozzle print head (the four bases plus the P–T solution) capable of producing single-picolitre droplets has been developed which can deposit 976,000 30 μm features in a 1 × 1 cm area (or ∼5 million features on a standard microarray plate).

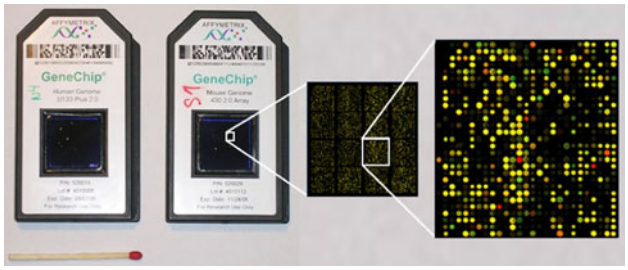

Fig. 1 Two Affymetrix microarray GeneChips® fabricated by photolithographic synthesis on quartz substrates, with matchstick for comparison. The Human Genome U133 chip (*left*) contains 1 million DNA probes. Magnified post-hybridisation images of probe spots (*insets*) show relative levels of expression of two analytes labelled with different (*red* and *green*) fluorophores. High intensity spots (*yellow*) indicate expression of both analytes. Reproduced from http://commons.wikimedia.org/wiki/

To perform an assay, the analyte is introduced and allowed to hybridise, followed by a washing step to remove unhybridised analyte. Then, a fluorescent label functionalised with one of the same probes is injected, which binds to the now immobilised analyte. This type of detection is known as a sandwich assay; alternatively, the fluorophore can be attached to the analyte itself and the last hybridisation step can be omitted. The array is then scanned by a laser and imaged by a CCD camera, and the probe is identified by the coordinates of the fluorescing feature. Microarrays are commonly used for gene expression studies; with spotted or cDNA microarrays the above procedure is usually done simultaneously with two samples from different sources (e.g. DNA from normal and mutant cells) which are labelled with two different fluorescent dyes, such as Cy5 (green) and Cy3 (red). The two samples are both hybridised to the array, which is scanned with red and green lasers and the two resulting CCD images are combined to show which genes are expressed most in the normal cells, which in the mutant cells, and which are equally expressed in both. These types of studies can only provide relative levels of expression, but with the development of oligonucleotide arrays, probes were designed to provide an estimate of the absolute levels of gene expression. Microarrays have been used in the last

[1] 'Traditional' DNA microarray technology is widely considered to have been developed at Stanford University, whereas the 'DNA chip' was pioneered by Affymetrix Inc. under their GeneChip® trademark, although a recent article by Ekins and Chu [37] seems to provide commonly forgotten facts about the origins of microarrays. This paper will refer to the two kinds interchangeably.

decade to study gene expression in *Saccharomyces* yeast [28] and in human leukaemia [55] and B-cell lymphoma [1].

Although microarrays have the advantage of being massively parallel, there can be problems with their accuracy for sequencing applications due to the logarithmic increase with probe length in the probability of obtaining probes which have incorrect or missing nucleotides.

Also, the selectivity of microarrays depends on factors such as the ratio of the concentration of analyte in the sample to the binding constant for the particular reaction, requiring extremely rigid user protocols [18]; extensive user expertise is also needed to interpret the fluorescence images, so it is difficult to both automate and extend the detection capability. Considerable image processing is also necessary, as to make measurements robust against intensity variations across the feature area, each feature must consist of at least 50 pixels, each of which must be scanned individually by a laser spot which must itself be size-matched to the pixel to avoid blurring of the image.

2.2 Sanger sequencing

Since it was invented by Sanger in 1975 [147, 148], chain termination or Sanger sequencing has been the 'gold standard' of DNA sequence decoding for its reliability and accuracy. The unknown sequence (the analyte) must first be purified and amplified, either by cloning in bacteria or by PCR [118]. A modern Sanger-based capillary electrophoresis instrument can sequence a read of up to 700–1000 bp from each of 768 DNA samples in parallel in an hour to PHRED 20 standard (a figure of merit for sequence data quality equivalent to 99.4% read accuracy) [102].

The Sanger method's accuracy means that it is still the main generator of high quality sequence information, particularly for de novo sequencing applications; despite this, it suffers from a number of problems. It shares the same problems as PCR, namely extreme sensitivity to contamination by (for example) RNA and foreign DNA, and to binding of the primer sequence to more than one site, leading to reading of more than one subsequence. It cannot also resolve secondary structure in the DNA (i.e. loops), which causes spurious bands to appear in the fingerprint and requires careful sample preparation. It is limited to reads of no more than 1000 bp because of the geometrical decrease with read length in the probability that the terminators will be incorporated, as well as the fact that gels and capillaries have a finite practical size and resolution. Although the sequencing itself is fast, the process of preparing samples for sequencing is long and exacting. Finally, the requirement to provide a separate gel lane or capillary for each analyte makes it difficult and expensive to extend the detection capability and throughput to the levels required for whole genome sequencing.

2.3 Beyond the Sanger method

The limitations of the Sanger method in terms of speed and cost therefore motivate the search for a technology that will maintain its accuracy, but with the potential for massively parallel functionality and throughput of hundreds of millions of bases per sequencing run. Such next-generation sequencing methods fall into two categories: sequencing-by-synthesis, which determine the sequence of the target base by base as it forms from the component nucleotides, and signature-based sequencing, which identify the sequence from a measurement of the target as a whole, which is then referenced against a database of signatures from known sequences. The main bottleneck to any DNA sequencing technology, now or in the future, is sample preparation; specifically, the production of enough copies of high-quality, pure target DNA to allow detection with high signal-to-noise ratio. This has been done in the past by PCR; new sequencing efforts depend on the ability to massively parallelise PCR. The most enthusiastically adopted approach is clonal amplification, which simply involves spatially localising each of the sequences to be identified on a solid substrate and then performing a series of conventional amplification steps. This creates a large number of isolated islands of DNA known as 'polonies' [113], each containing only one sequence. Clonal amplification methods include confining the templates with acrylamide gel which prevents diffusion of DNA [113] and BEAMing (beads, emulsion, amplification, magnetic) [33] in which an aqueous solution–oil emulsion is used to split a mixture of functionalised magnetic beads, free nucleotides, and a library of templates into millions of isolated droplets (ideally one bead and template per droplet) in which the template is amplified on the bead and collected for sequencing by magnetic separation.[2]

2.3.1 Pyrosequencing

The pyrosequencing application was first reported by Nyren in 1987 [123] and demonstrated for DNA sequencing in 1996 [143]. The DNA fragment to be sequenced is hybridised to a sequencing primer and immobilised to the substrate, then incubated with a cocktail of the enzymes DNA polymerase, ATP sulphurylase, luciferase and an enzyme such as apyrase which breaks down free nucleotides. The four base nucleotides are then added in a predetermined order; if the added nucleotide can form a base pair to the analyte, it is incorporated by the DNA polymerase and pyrophosphate is released. The ATP sulphurylase converts the pyrophosphate to ATP, which binds to the luciferase to

[2] For more information on amplification methods and related issues, we refer to [154] and references therein.

generate light. If the added nucleotide cannot bind to the analyte, it is quickly broken down by the apyrase. The next base can therefore be added and the process repeated. Although this method is both fast and accurate, and highly suitable for multiplexed assays, the reagents are expensive and must be frequently refreshed. Pyrosequencing also has some inherent limitations which usually restrict it to determination of sequences of 30–40 bases, although Margulies et al. [102] reported in 2005 a method now known as '454' involving a pyrosequencing reaction in an array formed from wells 44 μm in diameter and 55 μm deep etched into the ends of a bundle of 1.6 million optical fibres. By adsorbing the DNA onto 28 μm beads (and the sulphurylase and luciferase onto smaller beads), the team were able to extend the maximum read length of this sequencing-by-synthesis method to over 100 bp. This enabled them to sequence the 580,069 bp *Mycoplasma genitalium* genome at a throughput of 25 million bp in 4 h with an accuracy of 99.96%, compared to the published sequence for this genome [46]. The short read length in itself does not prohibit sequencing of entire bacterial genomes; in fact, the ease of oversampling afforded by the throughput of this system compared to Sanger sequencing allows for greater accuracy with much less effort. Read length has recently been increased to around 240 bp by researchers at 454 Life Sciences, and error rates decreased from 4% to 0.5%; however, this read length is still much shorter than those required to span homopolymer repeats (e.g. AAAAA...) in large (i.e. mammalian) genomes, and error rates of even 0.01% will still lead to hundreds of thousands of errors in the highly non-random human genome.

2.3.2 *Four-colour sequencing*

The main disadvantage of pyrosequencing in terms of speed (though not necessarily throughput) is that the pyrophosphate luminescence signal appears the same whichever base hybridises to produce it, meaning that '454' and similar technologies will always need to add the four bases individually. A sequencing run could be done more quickly in parallel by adding all four bases at the same time. Four-colour methods achieve this using four different fluorophores, each of which identifies one of the bases. A commercially available system of this type was developed by Solexa (now Illumina); its 1G Analyzer uses a slide as the substrate and amplifies templates by alternate double-stranding and denaturing of the templates [14]. The fluorescent label is attached to its nucleotide by a highly developed 'reversible terminator',[3] which blocks other nucleotides from being incorporated by polymerase to the growing complementary template, but which can be removed under mild conditions after each round of fluorescence imaging. Applied Biosystems offer a slightly different product which amplifies using clonal amplification on beads. The SOLiD system, based on work by Church et al. [155], uses DNA ligase to incorporate fluorescently labelled oligomers, which are composed of random bases except in a specific 'query' region, which has one of the four possible base substitutions. Ligation-based annealing offers improved discrimination against non-complementary or missing nucleotides compared to polymerase incorporation, and does not require extensive engineering of the properties of both the terminators and the polymerase, but other factors limit the template length to only 20 bp for now.[4] A promising third variation on four-colour sequencing has been developed by VisiGen Biotechnologies [157], based on single-pair FRET. This phenomenon allows emission from one fluorophore (the donor) to excite a second with an overlapping absorbance spectrum (the acceptor) by a long-range dipole–dipole coupling. Because FRET is sensitive to molecular rearrangements at the 1–10 nm scale, it has proved very popular in detecting DNA hybridisation, particularly when the acceptor is insensitive at the wavelength required to excite the donor. VisiGen exploit this effect by using a donor on a modified DNA polymerase to report both incorporation and identity of dNTPs labelled by four different acceptors. By making arrays of polymerase molecules, each of which will sequence a single template, VisiGen estimate sequencing speeds of 1 Mbase/sec per array, although extensive modification of both polymerase and nucleotides is required.

2.4 Signature-based bioassays

The methods described above are massively parallel and can be fast and accurate, but further improvements are required, such as longer templates which are essential for bridging long homopolymer repeats, a particular problem for the human genome. However, identification by synthesis techniques is not suitable for detection of pathogens or disease markers. Furthermore, the onerous sample preparation techniques, including amplification and purification of the sample, do not match well with the requirements of clinical diagnosis or biodetection in the field, which must measure a panel of analytes in a variety of media (e.g. groundwater, urine, saliva etc.). Therefore, very recent efforts have concentrated on developing multiplexed biodetection techniques which rely on large combinatorial

[3] Illumina's terminators and method of removing them is proprietary, but for information about a similar technology we refer to [76].

[4] For a review of highly parallel synthesis-based assays, see [42] and references therein.

libraries of complete biomolecular probes. However, such methods must find a way to distinguish individual binding events, and obtain a detection signal from each which specifically identifies it. This presents a formidable problem for both encoding and detection.

Some biomolecular identification methods use a spatially indexed array of probes (as in a microarray) and attempt to detect the binding events directly. Such label-free methods include measuring the deflection of functionalised nanoscale cantilevers [71] due to the extra mass of biomolecules (in the attogram range) or the change in the conductivity of a suspension of analyte, as molecules bind via an oxidation reaction to probes immobilised between the electrodes of an electrochemical cell [27, 38]. A variation on this amperometric detection is cyclic voltammetry, which applies a sawtooth voltage across the working and counter-electrodes to induce cycles of oxidation and reduction; frequently an electrically active molecule [165] or metal nanoparticle [130] is attached to probe or analyte to increase the signal. Capacitance and impedance measurements in solution [15] have been used for electrical detection of DNA hybridisation, and recently a thin-film FET has been used to detect DNA hybridisation via the change in gate capacitance of the FET, as natively negatively charged DNA binds to probes immobilised on the gate electrode [40].

However, a different approach to bioassay technology has adopted microfabricated labels of sub-micron to sub-millimetre size, each of which carries a detectable signature specific to the single species of probe with which it is functionalised [125]. Identification of the target or analyte then occurs by detecting the presence or absence of some minimum number of a particular population of labels during binding. Such labels act as a mobile substrate for the probes, and promise very high throughput when combined with microfluidic flow cells [39], allowing for three-dimensional, solution-phase hybridisation kinetics and providing a convenient way to confine reactions and transport reagents. Labels of this type have been realised in several forms, including ensembles of Raman tags [23] or encapsulated quantum dots (QDs)[5] [34, 62], identified by their specific emission wavelengths. 'Barcode'-like labels have been developed in the forms of fluorescent polystyrene microspheres selectively photobleached with encoding patterns by a high-power laser [21] and nanowires containing regions of low and high reflectivity metal [120] (Fig. 2a, b). Other, image-based labels include polymer particles graphically encoded by sequences of extruded dots [41, 137] (Fig. 2c) or by the diffraction patterns of overlapping etched gratings [10, 50].

Generally, the designers of labels intended for high-throughput, multiplexed detection have concentrated on optical encoding and detection methods like those previously mentioned. Fluorescent encoding in particular has become the current dominant technology in the field of molecular identification. However, fluorescent encoding suffers from a number of disadvantages; strategies to minimise autofluorescent background impose constraints on the portability of the detection system and sample preparation. For example, total internal reflectance fluorescence (TIRF) detection [4] diverts the majority of the excitation light by total internal reflection through the edge of the substrate and collects only the emitted fluorescence in transmission; this method requires both an intense, collimated light source (usually a laser) and a transparent substrate. Fluorescent molecules also tend to be expensive and subject to photobleaching over time; QDs have long fluorescent lifetimes but remain difficult to manufacture and passivate reliably [108]. More fundamentally, multiplexing is limited both by spectral overlap between fluorophores and by interference between binding signatures used to verify probe functionalisation of the labels and hybridisation between the probes and the targets, and encoding signatures used to identify the probe (and thus the target). Graphical methods solve this problem by using fluorescence only for hybridisation confirmation, but still require imaging of the label with an expensive and non-miniaturisable high-resolution CCD, with the associated disadvantages of non-real-time image analysis and data storage issues known from microarray methods.

3 Magnetic labels for bioassays

The first magnetic bead-based bioassay was suggested by Kriz et al. in 1996 [81], in which an inductive coil was used to measure the change in magnetic permeability of a gel due to specific binding of functionalised beads. In contrast, Baselt et al. [11] suggested in the same year that specific binding of beads could be detected by the deflection of piezoresistive cantilevers in a magnetic field, and by magnetic microsensors in 1998 [12]. This section will introduce magnetic beads and nanoparticles, and provide an overview of the preparation required to functionalise their surfaces for biomolecular attachment.

3.1 Commercial microbeads

There are hundreds of functional magnetic microbeads available from companies such as Invitrogen, Micromod and BangsLabs with a plethora of chemical and biological

[5] QDS are colloidal nanocrystals of substances such as CdSe, CdS, ZnSe, CdTe and PbSe, which emit highly monodisperse radiation when stimulated by UV light [108].

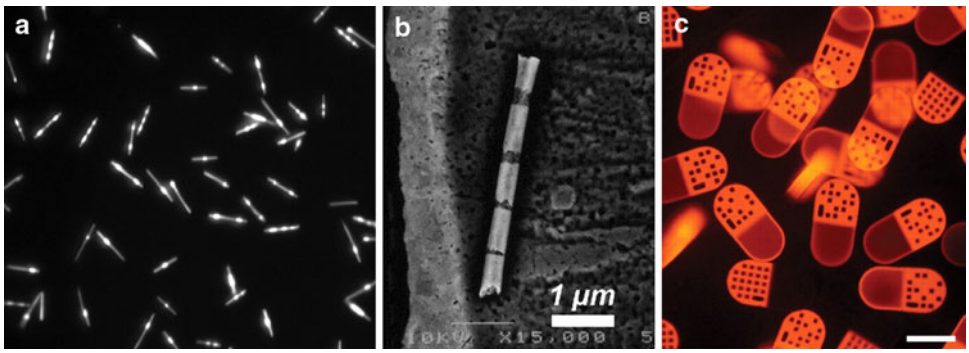

Fig. 2 **a** 4.5 μm Long metallic barcodes produced by sequential electrochemical deposition of Ag and Au. Under illumination by 430 nm UV, Ag segments show much higher contrast than Au segments. The nanowires in the image have between 0 and 9 Ag segments. **b** SEM image of a nanowire barcode, showing the 550 nm Au segments between Ag segments of length 240, 170, 110 and 60 nm (top to bottom). Reprinted from [120]. **c** Functionalised encoded microparticles fabricated by continuous-flow lithography in PEG. Scale bar represents 100 μm. Reprinted from [137]

surface coatings including amine, carboxyl, epoxide, hydroxyl, streptavidin, polythymine (for polyadenylated DNA), proteins A or G and a variety of antibodies. These microbeads are usually superparamagnetic, to avoid agglomeration, and consist of magnetic nanoparticles (commonly Fe_3O_4, Fe_2O_3 or CrO_2) dispersed in a silica or polymer matrix. As such they provide a convenient mobile substrate for performing biochemical reactions. As labels, magnetic beads possess several advantages. First, their magnetic properties are very stable over time and are generally not affected by reagent chemistry or exposure to light. Second, magnetic background in biological samples is minimal, since these are composed predominantly of diamagnetic molecules, and even large ($\leq$ 10 T) magnetic fields are compatible with biochemical processes. Finally, the stray magnetic fields from the beads, as well as externally applied field gradients which can be used to generate forces on the beads to remotely manipulate them, are not screened in an aqueous biological environment. These properties have therefore made magnetic beads a very popular choice of label/carrier for researchers working in μTAS due to the ease with which miniaturised magnetic detectors can be fabricated and integrated into detection systems using well-characterised techniques from the semiconductor processing industry. Another attractive feature of magnetic beads from the point of view of biological applications is the fact that they can be made fluorescent by the incorporation of QDs or dyes into the bead matrix, enabling direct comparison and cross-referencing with exclusively fluorescence-based methods of biodetection [119].

These beads have found application in a variety of immunoassays, molecular and cell biology applications including use in standard separation and purification procedures. However, none of these applications require careful control of the magnetic characteristics, and as a result, commercial beads typically have a wide distribution in sizes and saturation magnetisations, even within the same batch. This makes them unsuitable for quantitative magnetic assays based on measuring the number of bound beads or as distinguishable labels based on their magnetic moment. Our simulations have shown that only four or five commercial magnetic beads of different size can be distinguished magnetically [64]. Despite these drawbacks, their wide availability has made them a popular choice for testing of magnetic biosensor platforms.

3.2 Magnetic nanoparticles

Researchers working in biomedicine and on biosensor platforms have therefore begun to examine the potential of magnetic nanoparticles, on the scale of 5–150 nm, for biological labelling, drug targeting, hyperthermia and as MRI contrast agents. For a recent review of magnetic nanoparticles employed in these and other biomedical applications the interested reader is directed to [16]. There are a plethora of synthesis and coating strategies, and these are covered in more detail in a recent review article [142]. Therefore, here we will only touch on the basic concepts of magnetic nanoparticles for use in biomedicine.

Despite the often more favourable magnetic characteristics of cobalt and manganese ferrites, these are not well established due to concerns over their toxicity. However, if encapsulated or coated appropriately this toxicity can be significantly reduced, meaning they are a hot prospect for future development. Magnetite (Fe_3O_4) and maghemite (Fe_2O_3) are the most used precursors for magnetic nanoparticles, partly due to the ease with which they are formed. The most established method is co-precipitation from a basic aqueous solution (NaOH or $NH_3{\cdot}H_2O$) reaction of Fe^{2+} and Fe^{3+} salts [106, 115]. The size and shape of these nanoparticles can be tuned by controlling the pressure,

temperature, pH and ratio of the salts [159]. Depending on the application, the size of the nanoparticle is important, e.g. particles < 30 nm exhibit larger specific absorption rate values for hyperthermia applications [74]. However, their surface properties are as, if not more, important.

The surface needs to provide:

- Biocompatibility—non-toxic or fully encapsulate any toxic material.
- Monodispersity—the particles should be stable and not aggregate in specific solvents.
- Functionalisation—the particles need to have a high efficiency for binding target molecules or being taken up by specific cells.
- Non-specific binding should be minimised—for the case of DNA, electronegative groups such as COOH have proved useful.

The first step is usually to coat the nanoparticles with a polymer of some kind, often dextran or oleic acid which allows the nanoparticles to be stored in a stable suspension. These coatings can then either be further functionalised or swapped via a ligand exchange reaction. For instance, Lee and Harris [94] used ozone to cleave the oleic acid double bond forming carbonyl and carboxyl surface groups to increase the solubility in polar solvents. Another group [54] has shown that polydentate di- and tri-alpha-hydroxyacids, such as tartaric and citric acids exhibited stronger binding to Fe_3O_4 nanoparticles than simple alcohols/carboxylic acids that were prone to dissociation.

Another method is to use a core–shell strategy where the magnetic nanoparticle is encapsulated in a silica [70] or gold shell. Further functionalisation of gold coated nanoparticles and other surfaces usually proceeds via the growth of self assembled monolayers.

3.3 Self assembled monolayers

To grow a self assembled monolayer (SAM) we need an (usually) anionic ligand molecule, which will generally take the form of an alkane chain with a soft/hard 'head group' chosen to bind strongly with a soft/hard metallic surface and will often displace other adventitious surface absorbates to form a regular, reproducible structure. The other end of the alkyl chain has a 'terminal functional group' that can then be further modified by covalent chemistry.

The most well-studied systems involve alkanethiols grown on Au surfaces [8, 9, 78, 79, 104, 117, 122], although sulphur also shows a strong affinity towards the other noble/coinage metals, including Ag [9], Pt, Cu, Hg and Pd. Au is most often chosen due to its inertness and resilience to oxidation—so we shall start by discussing this system. Although there are several reports of other SAMs forming on various metals, including disulphides on both Au and Ag [63, 66], isocyanides on Au and Pt [66, 104] and carboxylic acids bind selectively to metal oxides (hard–hard pairings), including Al [9, 92] and Ni [13, 138, 144, 160]. A few groups have electrodeposited Ni–Au composite nanowires and functionalised the different segments simultaneously with a mixture of carboxylic acid and thiol chains [92]. This opens the door for greater flexibility, such as having a fluorescent label for tracking and a biological probe on different sections of the same tag. Organosilanes have also been of interest, particularly in the semiconductor industry, and may offer covalent attachment with a SiO_2 [101, 124] or Ta_2O_5 [128] surface, although this has not been conclusively shown and it is currently believed that most of the covalent chemistry occurs between adjacent monomers forming lateral siloxane (–Si–O–Si–O–) bonds.

3.3.1 Thiol and disulphide SAM functionalisation of gold

A range of methods are used to coat nanoparticles with Au, either as a core–shell model [171] or as composite gold/iron–oxide nanoparticles [152]. Microcarriers incorporating gold surfaces include electrodeposited nanowires [121] and our own magnetic barcodes—both polymer-encapsulated [68] and electrodeposited [127]. Much work has been done with thiolated single-stranded DNA (ssDNA) binding to Au by other researchers [107, 135], and within our group to attach probe DNA to planar tags containing a gold plate [68]. Both thiols and disulphides can be deposited from solution or in ultra-high vacuum conditions, [122] and very little is conclusively known about the absorption mechanism, but it is expected that the chemisorbed S atom fills the holes between three Au atoms on a (111) surface to provide the maximum coordination environment forming a $(\sqrt{3} \times \sqrt{3})R30^\circ$ constructed SAM. The absorption mechanism for thiols and disulphides is subtly different and has important consequences. From a mixed solution thiols are physisorbed preferentially ($\sim$75:1) due to their lower steric hindrance [7]. However, chemisorption proceeds more readily for disulphides than thiols, because there is a large energy barrier that must be overcome for thiols to lose a hydrogen atom and form a thiolate anion. The thiolate is readily formed in the case of disulphides from the dissociation of the S–S bond, and is remarkably thermally stable once chemisorbed, having an activation energy of desorption of $\sim$28 kcal/mol [122]. Final analysis of the SAMs formed from either the thiol or disulphide shows no chemical difference, which suggests that the thiolate anion is eventually formed for thiols as well. However, this is only the case for SAMs deposited from solution, suggesting that the presence of adventitious oxygen may aid the deprotonation of the physisorbed thiol.

Our group has used a disulphide molecule (fabricated in house [127]) with NHS head groups to grow a monolayer

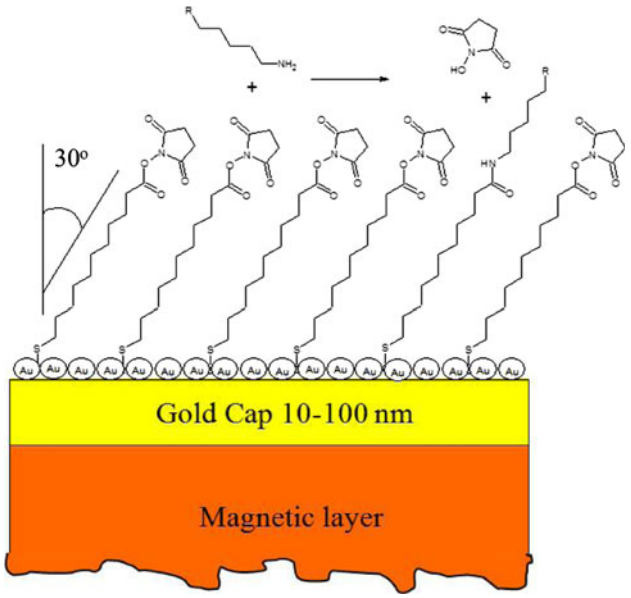

Fig. 3 Schematic of the self-assembled monolayer with functional NHS head groups, reactive to primary amines, such as NH_2 modified ssDNA

on gold capped electrodeposited pillar tags (Fig. 3). The same monolayer has been grown by other groups using a two-step method [47, 80, 132, 166]. First they deposit an 11-mercaptoundecanoic acid, (MUA), to form the SAM and then use an 1-(3-dimethylaminopropyl)-3-ethylcarbodiimide/NHS activation method to immobilize biomolecules. The advantage of this method is that the NHS group is labile and will readily hydrolyse in water/air at room temperature (RT).

3.3.2 Non-specific binding

Non-specific binding is a recurring problem in hybridisation assays and there are two main factors attributed to increased non-specific binding to SAMs—hydrophobicity of the monolayer and electrostatic interactions (particularly in the case of carboxylic acids that can form ionic bridges with the phosphate backbone of DNA [158]). To combat this, several groups have researched using a mixture of SAMs [47, 89, 91], using a hydroxyl terminated SAM that provides a hydrophilic background, with a 2–10% population of the SAM to be used for covalent binding. Using hydrophilic PEG chains has been shown to reduce non-specific binding compared to simple alkyl chains [47, 89]. It is also important to note that they found that reducing the content of the binding SAM was not significantly detrimental to the overall yield for their applications. In fact Lahiri et al. [91] found that a 2% incorporation of the binding SAM was enough to bind 60% of the carbonic anhydrase protein compared to that bound using only the binding SAM. This was believed to be due to geometric factors and the size of the protein molecule, which covers over 60 thiolates in the SAM. Whitesides' group [6, 8] have reported interesting results on the growth of mixed SAMs on Au from solutions containing a mixture of thiols with different length alkane chains. They found that the relative absorption processes were under thermodynamic control rather than kinetic. Simply put—the more soluble (i.e. stable) the SAM molecule is in the solvent, the less abundant it is in the monolayer deposited on the surface.

3.3.3 Tridentates

The exact binding mechanism of SAMs is not understood conclusively, but covalent bonding is unlikely [99, 126], and as such SAMs can be displaced by other thiols, an event known as ligand exchange. This is particularly problematic when further functional steps involve thiol groups that could interfere with the SAM itself, decreasing yield and reproducibility. In reaction schemes where this is the case it is favourable to use molecules with three thiol 'legs' to increase the binding strength of the SAM, which no longer shows any significant ligand exchange [169]. The surface area occupied by these tridentates is also comparable to the single-thiol compounds, experiments suggest 25–30 $Å^2$ only.

3.4 Epoxide chemistry

The epoxy group owes its increased reactivity to its highly strained three-membered ring structure, effectively increasing the electrophilicity of the least substituted carbon. Epoxides react strongly with nucleophiles, and can be catalysed by either acid or base. A two-step functionalisation procedure was developed by researchers in Southampton, who added a Jeffamine^{TM} spacer in MeCN at 65°C with overnight stirring [25]. They found that although shorter spacers attached with a higher yield, the proceeding step benefited significantly from being further from the surface. Another group have converted the surface of the

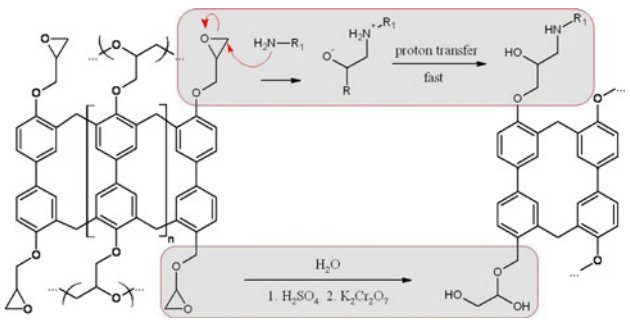

Fig. 4 SU8 functionalisation schemes (*top*) direct nucleophilic attack of the epoxide ring; (*bottom*) oxidation to hydroxyl groups as in [75]

polymer SU8 (Microchem) to hydroxyls using sulphuric acid with a $K_2Cr_2O_7$ catalyst with the reaction shown in Fig. 4 [75].

Epoxides are stable in water at neutral pH, and for efficient nucleophilic attack a high pH is recommended—pH 9 for amines and pH 11 for hydroxyls [65]. Direct coupling of ssDNA (with and without 5′ amine modification) onto SU8 and subsequent hybridisation has been reported [103] using a 1 M potassium phosphate buffer (pH 7.4). The researchers believed this to be covalent bonding, but were unclear whether this was with the epoxide groups since pre-treatment with ring opening reagents, such as ethanolamine, did not influence the results. Wang et al. have reported a highly efficient scheme for oxidation of the surface epoxides to hydroxyls (similar to that shown in the bottom panel of Fig. 4). They used a cerium (IV) ammonium nitrate (CAN) catalyst (0.1 M) in 1 M HNO_3 to soak the SU8 for 16 h [13].

4 Magnetic bead-based biosensors

Research in this area has developed along three general directions: first, synthesis of magnetic beads with desired magnetic properties that can be functionalised with a high degree of specificity as discussed above. The second has focused on development of high-precision on-chip electrostatic or magnetic field gradient architectures ('striplines') capable of manipulating functionalised single magnetic beads, as well as the microfluidic circuits for controllable transfer of biomolecular probe–bead complexes to desired areas on the biochip. The third area, on which this review will concentrate, is development of biocompatible solid-state sensors for quantitative detection of single magnetic beads.

Since the work by Kriz et al. [81] much work on magnetic bead assays has been carried out [109], the majority of which employ magnetoresistive or Hall sensors. Other, non-local detection methods have been employed for magnetic beads, notably inductive sensing systems with more sophisticated detection electronics [93] and AC susceptibility measurements [29], which measure the change in the Brownian relaxation of the beads as analyte molecules bind and increase the bead's hydrodynamic radius.

In their approach to actual biomolecular identification, magnetic biosensors tend to mimic previous technologies; arrays of sensors have been proposed [12], the surface of each of which is functionalised with a different probe molecule, just as in the conventional microarray. Sandwich or binding assays are also extensively used, performed in the same way with the simple substitution of a magnetic bead for the fluorescent label [27, 48, 58, 150].

4.1 Hall effect biosensors

Discovered in 1879 [61], the classical Hall effect is a manifestation of the Lorentz force acting on charge carriers in a material exposed to a perpendicular magnetic field and carrying an in-plane current. Hall effect devices have been used as magnetic field sensors both in the laboratory and in industry (mostly for position and proximity sensing) for decades. The most common geometry is the Hall cross

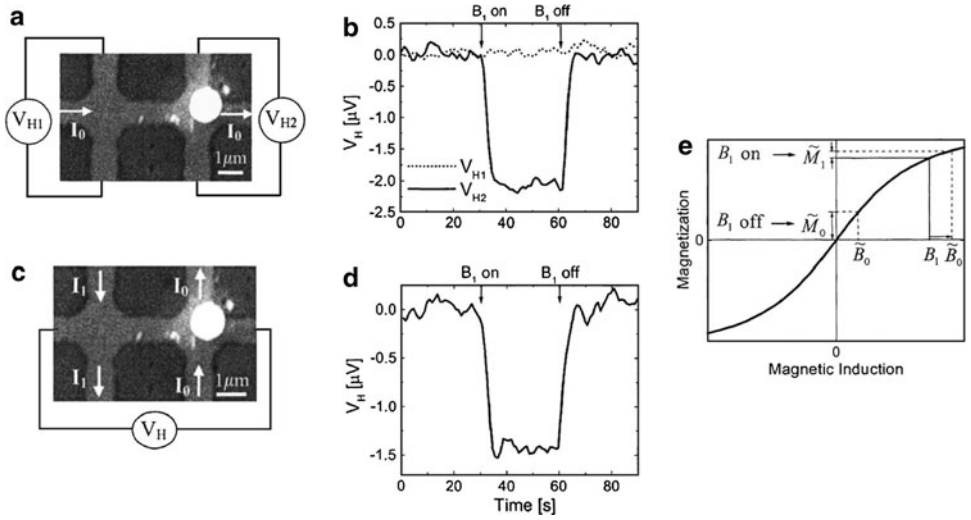

Fig. 5 **a** SEM image showing Hall crosses with and without a 1.2 μm bead; both sensors are biased with $I_0 = 40$ μA. **b** AC Hall voltage vs. time for the two Hall crosses in (b). $\tilde{B}_0 = 2.13$ mT rms at 622 Hz and $B_1 = 6.1$ mT. **c** The Hall crosses in (**a**) are now configured as a gradiometer, where $I_0 = 30$ μA and $I_1 = 31.45$ μA; the resulting AC Hall voltage vs. time is shown in (**d**), where $\tilde{B}_0$ is increased to 2.35 mT. **e** Typical Langevin response of a superparamagnetic bead with a sketch of the physical principle of the detection method, where $\tilde{B}_0$ and $\tilde{M}$ are rms values of the AC applied field and resulting AC magnetisation respectively. Reprinted from [110]

(Fig. 5a, c), a four-terminal device in which the current is injected through two terminals and the voltage measured orthogonal to the current flow through the remaining two. In zero magnetic field this voltage is zero; in the presence of a perpendicular magnetic field B, the resulting Lorentz force causes charge carriers to accumulate along the sides of the device parallel to the current I. This charge accumulation in turn generates an additional electric field perpendicular to the current flow and thus a voltage across the sensing terminals. This Hall voltage, V_H is given by

$$V_H = R_H IB, \tag{1}$$

where the Hall coefficient $R_H = 1/ne$ for a two-dimensional electron gas (2DEG) system with 2D electron density n and $e \cong -1.6 \times 10^{-19}$ C is the electronic charge.

Magnetic bead detection using Hall crosses is usually performed using an AC phase-sensitive method [17], which exposes bead and sensor to a small perpendicular AC field $\tilde{B}_0$ and measures the Hall voltage at the first harmonic with a lock-in amplifier. A larger DC field B_1 is then applied in the same direction; due to the Langevin behaviour of superparamagnetic beads, an increase in the DC magnetisation of the bead lowers both its susceptibility (the slope of its magnetisation curve) and its AC magnetisation as shown in Fig. 5e. This manifests itself as a drop in the Hall voltage when B_1 is applied, but only if a bead is present over the sensor, as the linear behaviour of the Hall sensor itself means that its AC magnetisation is the same regardless of its DC magnetisation state. Figure 5a illustrates work done by Mihajlović et al. [110], and shows an InAs quantum well-based Hall cross with 1.0 × 0.9 μm sensing area with a single 1.2 μm diameter paramagnetic bead and an identical, empty cross; Fig. 5b shows a comparison of the responses of the two sensors. Only the cross below the bead shows the expected drop in the Hall voltage, whereas the empty cross is unaffected. A potential weakness of this method is the large offset from the direct response of the sensors to the AC field, which is typically orders of magnitude greater than the signal due to the bead; the traces in Fig. 5b are obtained using a zero offset on the lock-in amplifier. A potential solution uses two crosses as before in a gradiometer configuration, as seen in Fig. 5c, in which a reference current I_1 is applied to the empty cross in the opposite direction to the active sensor bias current I_0. By adjusting I_1 to zero the AC Hall voltage in the absence of the DC field, the offset is nulled effectively as seen in Fig. 5d. However, the measurement noise is visibly increased, as now both crosses contribute.

Phase-sensitive detection using InSb Hall crosses has also been demonstrated by Sandhu et al. [146], in which 2.8 μm diameter beads were detected using an AC excitation field now applied in-plane and a perpendicular DC field applied by a permanent magnet. In this measurement geometry, the Hall voltage is again measured at the first harmonic, but now increases when the DC field is applied if a bead is present over the sensor.[6] Comparison with concurrent magnetoresistive [12] and previous Si based Hall sensors [17], detecting similar particles, indicated that the 5 × 5 μm InSb Hall crosses displayed improved signal-to-noise characteristics as well as being capable of detecting smaller superparamagnetic particles due to the shorter distance between sensor and bead (∼250 nm). Improved devices with a higher magnetic field sensitivity were reported in Ref. [162] in which an array of such Hall crosses indicated the feasibility for multiplexed detection, while a 30 × 30 μm InSb sensor successfully detected 200 nm diameter particles. A recent comparative study on different materials suitable for Hall biosensors [145] concluded that sensors based on semiconductor heterojunctions, such as InAs-AlGaSb, show the highest sensitivity, particularly for the case that beads can be localised to the edges of the device which permits quantitative bead detection [83].

In summary, the Hall cross is attractive for biosensor applications due to compatibility with semiconductor industry materials and processes, simple and easily fabricated geometry, and potentially high sensitivity and magnetic field resolution, although it is not clear how well it would be able to detect ferromagnetic beads, which have hysteretic magnetisation behaviour.

4.2 Magnetoresistance-based biosensors

First measured by Lord Kelvin in 1857 [161], magnetoresistance (MR) is simply the change in the resistance of a material due to the application of a magnetic field. The size of the effect, the MR ratio, is always defined to be

$$\mathrm{MR} = \frac{\Delta\rho}{\rho} = \left(\frac{R_{\max} - R_{\min}}{R_{\min}}\right), \tag{2}$$

where ρ is the material's resistivity and $R_{\max}$ and $R_{\min}$ are the maximum and minimum measured resistances. Whether $R_{\max}$ is attained at high, low or zero applied field depends on the origin of the particular kind of magnetoresistance exhibited by the material (or the sum of several kinds). Bead detection based on MR follows closely ideas from Baselt and Miller (Fig. 6) in which the beads and sensors are exposed to external magnetic fields, in the plane of the sensor [97] or out-of-plane [12], which induces a magnetic dipole in the bead aligned to the applied field. In the out-of-plane case, the resulting stray

[6] It should be noted that this experimental procedure differs from that proposed in [17] for this geometry, which demands Hall voltage detection at the second harmonic, and requires a much lower DC field (4.6 mT as compared to 32 mT).

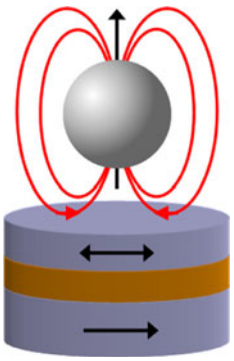

Fig. 6 Measurement geometry for MR bead sensing for beads externally magnetised out of the sensor plane

field from the bead projected onto the plane of the sensor follows a radially symmetric pattern with the maximum just within the 'shadow' of the bead and zero field directly below it. In contrast, the field in the in-plane case is mostly unidirectional and is opposite in sense to the applied field. In either case, the presence or absence of the bead modifies the effective applied field experienced by the sensor, and consequently alters the sensor's magnetoresistance, providing a detection signal in the form of a voltage change (in the case that the sensor is supplied with constant current).

$$B_{\text{bead}} = \begin{cases} \frac{3mz\rho}{(\rho^2+z^2)^{5/2}} & (H_z, \text{cylindrical coords.}) \\ -\left(\frac{m}{4\pi z^3}\right) & (H_x, \text{Cartesian coords.}) \end{cases} \quad (3)$$

However, the stray field from the bead declines rapidly with distance from the centre of the bead, as seen from Eq. 3 (cgs units) [36, 112] and so most MR sensors attempt to measure a large number of beads to obtain a high signal-to-noise ratio, usually through mass coverage of the sensor surface by a monolayer of beads. Unfortunately, such averaged detection methods are unsuitable for reading of bead libraries, where each bead is supposed to be functionalised with a different DNA sequence, and so must be sensed individually. Recent efforts have therefore moved toward single-bead detection by MR sensors size-matched or smaller [163], which ushers in the possibility of very fast, high-throughput assays suitable for applications such as affordable whole-genome sequencing. Such schemes are vulnerable to inaccuracy if beads are lost; an elegant approach suggested by Tondra et al. [164] and reported by Lagae et al. [90] and Graham et al. [56] involves directing the bead onto the sensor by magnetic field gradients generated by microfabricated current lines.

4.2.1 Anisotropic magnetoresistance biosensors

The resistance of a device made of ferromagnetic material can depend on the angle between the magnetisation and an applied current. Known as anisotropic magnetoresistance (AMR), this effect can be described by the relation

$$\rho(\theta) = \rho_{M\perp} + \left(\rho_{M\parallel} - \rho_{M\perp}\right)\cos^2(\theta), \quad (4)$$

where $\rho_{M\perp}$ and $\rho_{M\parallel}$ are the resistivities with the magnetisation perpendicular and parallel to the current, respectively, and θ is the relative angle between the current and magnetisation directions. According to this relation, the resistance is high when the magnetisation lies parallel to the current and low when the current and magnetisation are perpendicular, as generally $\rho_{M\parallel} > \rho_{M\perp}$.

The AMR effect offers much scope for tailoring the shape of the device to constrain both the flow of current through it and the magnetisation to obtain a desired resistance response.[7] Accordingly, the two biosensors reported which use AMR are a cross [35, 36] very similar to the Hall crosses previously mentioned and a ring [112]. The former consists of two crossed 60 × 10 μm bars of 200 Å thick $Ni_{80}Fe_{20}$ or permalloy (Py). A voltage is generated perpendicular to the current direction in response to an in-plane magnetic field, as the magnetisation of the active area rotates with respect to the current. By analogy with the Hall effect, this manifestation of AMR is known as the planar Hall effect, although the origin is quite different. The introduction and removal of droplets of magnetic beads produces voltage drops due to the field from the beads opposing the applied field. This mass-coverage sensor detects the combined fields of ~1.5 monolayers of 2 μm beads, and is interesting because it can be operated without any external field. As the sense current flows along the 10 μm wide central bar, it generates a relatively uniform field of ~4–6 Oe, which can magnetise the beads. The current must be relatively high (10–15 mA) but the stray field from the monolayer of 2 μm Micromer® -M beads (Micromod) in response is around 1.5 Oe, or 25% of the 'applied' field. The change in field is easily detected by this sensor design given the case of mass coverage and very low experimental noise (~250 nV) even under DC fields and currents.

The ring-shaped AMR sensor (outer diameter 5 μm, inner diameter 3.2 μm) is also fabricated in 200 Å thick Py and is designed to detect single beads; the bead (a 4.3 μm $Ni_{70}Fe_{30}$ sphere) is positioned over the ring using a modified atomic force microscope (AFM) cantilever. In a perpendicular field of 35 Oe, which is much smaller than that required to magnetise the Py in this direction, the induced radial field from the bead is used to rotate the magnetisation of the ring away from its circumferential zero-field configuration. This raises the AMR level relative to an identical reference ring which forms the opposite arm of a Wheatstone bridge; a standard lock-in technique

[7] An example is the 'barber-pole' sensor [82], which constrains the current to travel always at 45° to the dominant magnetisation direction in order to linearise the AMR.

measures the resulting AC voltage imbalance in the bridge at the second harmonic.

In both of these sensor designs, the available signal is limited by the small size of the AMR effect (~2% at RT [53]). Much greater MR values and better signal-to-noise may be attained by biosensors based on the giant magnetoresistance (GMR) and tunnelling magnetoresistance (TMR) effects.

4.2.2 Giant magnetoresistance biosensors

In systems composed of magnetically independent ferromagnetic regions separated by ultrathin (i.e. spin-conserving) non-magnetic spacers, measurements of the field-dependent resistivity can yield MR ratios at RT well in excess of 100%. This GMR effect was reported by Baibich et al. in 1988 in Fe/Cr superlattices [5], and independently in 1989 by Binasch et al. [19] in antiferromagnetically coupled Fe/Cr/Fe trilayers. However, the discovery by Dieny et al. in 1991 [32] of GMR in various uncoupled ferromagnetic/non-magnetic/ferromagnetic thin films inspired much research into design and optimisation of GMR multilayers,[8] particularly for hard disc read heads [131]. What was dubbed the spin-valve (SV) is easy to fabricate and relies on the GMR effect. This depends on spin-dependent scattering of electrons at the interfaces of the ferromagnetic layers, and thus on the relative alignments of the layer magnetisations. In the SV, ensuring that the magnetisation of one layer is free to rotate with the applied field while the other remains relatively pinned is now usually done by depositing an antiferromagnetic layer such as FeMn or IrMn next to the 'pinned' layer, in order to constrain its magnetisation via exchange coupling. For the simpler trilayer system, now called the pseudo-spin-valve (PSV), this can be done by controlling the relative thicknesses or compositions of the two layers. The highest sensitivity to the layer alignments and greatest MR is achieved when the sense current travels from top to bottom of the GMR stack, a geometry known as current perpendicular-to-plane (CPP). However, in practice devices based on this principle pose technological difficulties, because the CPP resistance of the device tends to be much lower than the contact resistance of the current/voltage leads. Most GMR sensors therefore use a current in-plane (CIP) geometry in which the electrons travel parallel to the layer interfaces; the MR is lower as only a proportion of the electrons experience any interface scattering, but both fabrication and measurement are simplified.

[8] Carefully designed multilayer spin-valves can have MR of over 20% [67]. Simple trilayer systems like those described here have MR percentages of $\leq$ 10%.

GMR biosensors, both sandwich- and spin-valve-based, fall mainly into two categories, using either mass-coverage or single-bead detection. The former kind include the first work done on GMR bead sensing [12]. Envisioned as a portable detection system for biological warfare agents, an array of 80 × 5 μm GMR multilayer strips on a 2.5 × 2.5 mm chip was used to detect 2.8 μm M-280 Dynabeads® (Dynal Biotech/Invitrogen) in a concept known as bead array counter (BARC). Each sensor would be functionalised with a different DNA probe and sandwich bioassays would be performed. BARC-II chips followed [111], in which the 64 sensors were arranged in groups of eight, each covering one DNA probe 'sensing zone', which were used to identify a DNA oligomer taken from the microbe *Franciscella tularensis* (FT). Analyte made of biotin-conjugated single-stranded FT DNA was introduced to a chip containing two zones each of DNA from FT, *Yersinia pestis* (YP), *Botulinum* neurotoxin B (BB) and a biotin-conjugated positive control (PC) designed to provide a measure of maximum signal. The signal from the FT-functionalised sensors was ten times that of the YP and BB zones and 75% of the positive control. Development continued on BARC-III chips, in which each GMR strip has been expanded into a serpentine trace covering a 200 μm diameter circle, to match the size of pin-spotted DNA probe sites [140].

Although these experiments showed that solid-state MR biosensing could provide selective detection of DNA targets, they did not address quantitatively the dependence of the sensor response on the number of beads on the sensor, or by extension the concentration of the target DNA. Further work on GMR mass-coverage bead sensors was performed by a group at the University of Bielefeld [150], who systematically measured sensor signal versus bead coverage for three different types of beads, as determined by SEM [151]. They showed a linear increase with coverage, despite polydispersity and clustering of the beads. Their sensors are a single strip of GMR superlattice material patterned into a spiral with a diameter of 75 μm, to cover one pin-spotted DNA spot, as shown in Fig. 7a. The same group also performed a DNA hybridisation assay with these sensors and compared their performance to fluorescence detection, in which curiously the concentration of probe DNA (rather than the target DNA) was varied in five steps from 16 pg/μl to 10 ng/μl and the same volume of each was spotted onto the sensors. Because the spots spread out to ~1 mm in diameter, the average value of seven to eight spots covered by specific probe DNA was taken and compared to unspecifically functionalised reference sensors. A standard sandwich assay was then performed by incubating the sensors with biotinylated complementary DNA for 12 h and then with either streptavidin-functionalised 0.35 μm magnetic beads or a fluorescent marker.

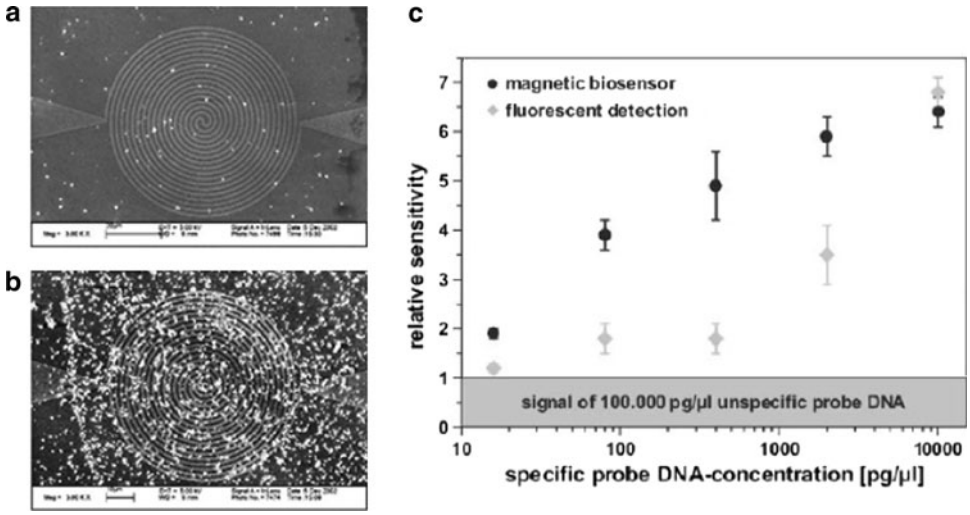

Fig. 7 SEM images of spiral GMR sensors after incubation with functionalised beads, showing level of bead attachment to sensors with **a** non-complementary and **b** complementary DNA. **c** Relative sensitivities (normalised to detection signal of non-complementary DNA) of bioassays based on fluorescent (*grey diamonds*) and magnetic (*black circles*) labelling and detection. Reprinted from [151]

The results, reproduced in Fig. 7c, show that while the magnetic assay is more sensitive at low concentrations than fluorescence, it shows a clear tendency to saturation. The magnetic results also do not reproduce the fluorescence results well except at very low and very high probe concentrations; the sensor output also increases by only a factor of three for a probe concentration range of three orders of magnitude. These reasons led Megens and Prins [109] to comment that the test measures the likelihood of DNA attachment, rather than the concentration of DNA in the sample.

Further work on mass-coverage GMR sensors has reported several successful magnetic bead-based bioassays including work by Freitas et al. on detection of DNA from genes associated with cystic fibrosis [59]. Their detection platform used a number of 2 × 6 µm SV sensors, which are functionalised with DNA probes containing a 50 bp region specific to the cystic fibrosis transmembrane regulator gene (CFTR). The 250 nm Nanomag®-D beads (Micromod) were magnetised in-plane by a planar permanent magnet as well as fields produced by 1 µm thick Al tapered current lines either side of the sensor. The system was soon improved by making the sensors U-shaped and larger to accommodate more beads, with similarly shaped striplines around them driven by an AC current [43, 44, 105] (Fig. 8a, inset). The group earlier reported real-time measurements of the progress of binding of functionalised beads to the sensor in liquid, as is required for a real application [56, 57]. By using optical microscopy, they were even able to correlate the signal to the arrangement of beads on the 2 × 6 µm sensors. Using just the 15 Oe DC in-plane magnetic field produced by the permanent magnet, the signals from one, two and four 2 µm Micromer®-M beads could be easily distinguished.

Detection of a single bead was achieved by Llandro et al. [98], who positioned a 4.5 µm diameter M-450

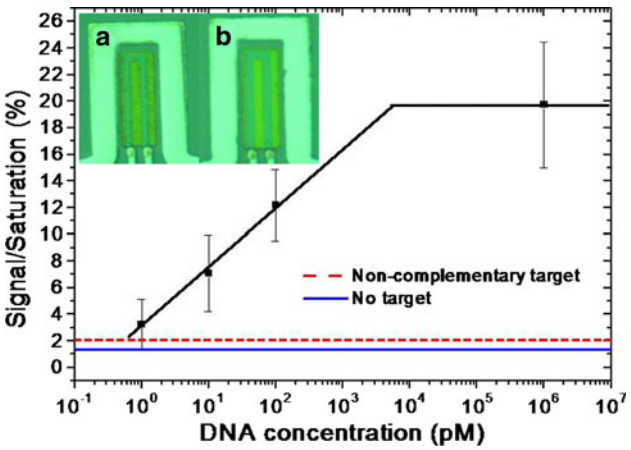

Fig. 8 Biological detection limit for single stranded DNA sequences encoding for the genomic region of the 16S ribosomal sub-unit of *E. coli*. The *straight lines* connecting the experimental data points are guides to the eye. Inset: Optical micrographs at 800x from individual sensors corresponding to (**a**) 1 µM target and (**b**) no target assay. Reprinted from [105]

Dynabead® in solution over a Py/Cu/Co PSV ring 4 µm in diameter with a 300 nm linewidth (MR ~1.4%). The ring was separated from the bead by a 150 nm thick layer of polymethylmethacrylate to protect the ring from the liquid, which reduced the maximum possible stray field reaching the ring. Measurements of the ring's GMR revealed an increase in the Py layer's switching field of 5 ± 0.2 Oe; by cycling the external field from saturation into the field window created by the increase, it was possible to completely prevent the ring switching in the presence of the bead. This was suggested as a route to digital identification of encoded beads, whereby the applied field required to null the ring's response would identify the bead by its magnetic moment.

Single bead sensing has also been reported by Wang et al., in whose experiments a single 2.8 µm Dynabead®

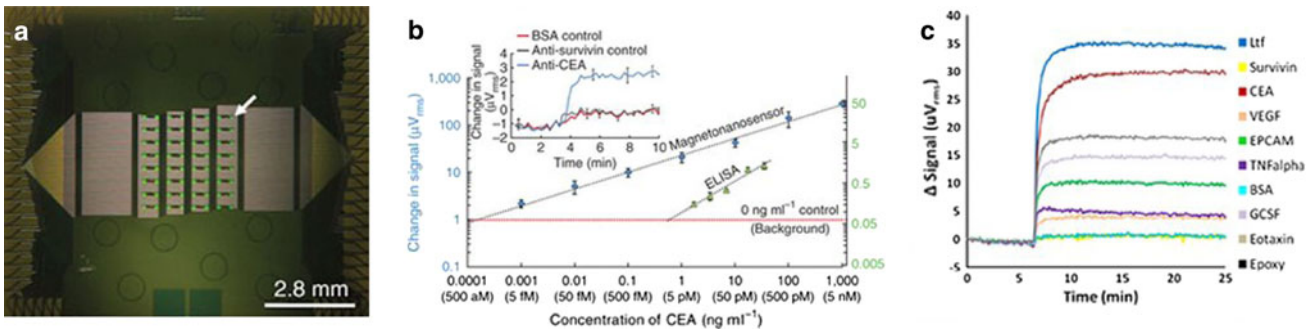

Fig. 9 **a** Image of magnetonanosensor chip with 64 sensors in an 8 × 8 array. The *arrow* indicates a single uniquely addressable sensor. **b** Comparison between ELISA and magnetonanosensor detection platform. *Inset* shows the real time response of the magnetic sensor to the addition of 5 fM CEA. **c** Real time binding curves of magnetic nanoparticles to detection antibody for each of eight unique biomarkers in a single reaction well. Reprinted from [52]

was detected by rectangular SVs (MR = 10.3%) [96]. A DC field H_b along the long axis of the sensor was used to magnetise the bead and a smaller orthogonal AC field H_t at 40 Hz to modulate the bead's magnetisation. The same group aimed to detect a single magnetite nanoparticle (10–20 nm diameter), which is the most appropriate size for functionalisation by just one strand of probe DNA. Progress towards this goal has recently achieved detection of a monolayer of oleic acid-coated 16 nm magnetite nanoparticles on a 1 × 0.3 μm SV [95], though the signal-to-noise level is only ~3, indicating that single-nanoparticle detection on this platform was not possible. By changing to a simpler detection system using only a single DC in-plane field and constant 1 mA current, however, signal-to-noise was improved to the point that a cluster of 23 nanoparticles could be detected [97], although the minimum detection limit was still 14 nanoparticles. The group recently showed [52] that the latest implementation of their antibody sandwich assay on GMR sensors (Fig. 9a) is capable of multiplexed detection of protein tumour markers in a variety of clinically relevant media down to attomolar level (Fig. 9c). They also performed a comparative study between their magnetic based biosensor to an enzyme-linked immunosorbent assay (ELISA) (Fig. 9b). The results show that the linear dynamic range for detection of the carcinoembryonic antigen (CEA) and lactoferrin by ELISA is constrained to two orders of magnitude in the picomolar range, whereas the magnetic assay covers six and five orders of magnitude upwards from the femtomolar range, respectively. Finally, a comparison between the two platforms based on quantitative protein detection indicate a similar ability to quantify the concentration of the protein HCG in an unknown sample.

4.2.3 Tunnelling magnetoresistance biosensors

A similar structure to a PSV or GMR multilayer replaces the non-magnetic metal spacer with an ultrathin insulating barrier, commonly Al_2O_3 or MgO. When this structure is operated in the CPP geometry, spin-polarised electrons are able to tunnel through the barrier, with total transmission determined as before by the relative angle between the polarisations of the electrons and the magnetisations of the top and bottom magnetic layers. This TMR effect was first reported by Julliere et al. in 1975 [77], but remained a curiosity until 1995, when high-quality ferromagnetic/insulating/ferromagnetic trilayer films were first successfully fabricated by Moodera et al. [116]. Recent work by Parkin et al. [51] and Yuasa et al. [170] has demonstrated TMR values of 150–350% at RT using variations on structures with CoFeB or Fe magnetic layers and an MgO barrier.

Although GMR sensors can detect single micron-sized beads with excellent signal-to-noise ratio, a compromise must be made in bioassay applications between the size of the sensor (which detects single beads most efficiently when the sensor and bead are size-matched) and the biomolecule binding capacity of the bead. Smaller (i.e. submicron to nanometre-sized) beads bind more easily to DNA, but it is increasingly difficult to fabricate GMR sensors which maintain a measurably high resistance at these sizes, due to their all-metallic structure. By replacing the non-magnetic metal spacer with an ultrathin insulating barrier, the magnetic tunnel junction (MTJ) avoids this problem. However, the challenges of making high-quality, ultrathin oxide layers and the necessary electrodes for CPP operation of MTJs, not to mention operating them in biocompatible liquids, have meant that few groups have adapted the MTJ for biosensing despite its potential advantages. Those that have reported bead sensing with MTJs have tended to purchase them from companies manufacturing memory chips or magnetic field sensors [60, 72] such as Micro Magnetics, Inc. However, Wang et al. [168] report fabrication of arrays of functionalised MTJs for biosensing, and workers at Bielefeld [22, 139] show a comparison of output from a 70 μm diameter serpentine

GMR strip and a 20 μm MTJ, both ~6% covered with 0.86 μm beads. The MTJ response was about four times larger than the GMR sensor signal. A review [49] comparing the two major MR based biosensors currently used to detect single molecular recognition processes concluded that the choice between MTJ (TMR) and SV (GMR) sensors cannot be based solely on the ability of the MTJ to detect weaker magnetic fields (10 to 20 times weaker than a similar area SV sensor). One has to remember that it is easier to manufacture CIP SV than CPP MTJ making the integration of the former into a biochip more effective. Moreover, the ability to detect ever weaker magnetic fields for ever smaller magnetic carriers requires a larger area MTJ while keeping the TMR value high, but the probability of pinholes reducing the TMR also increases with increasing area. Therefore, the choice between the two has to depend on the biological sensitivity required for a certain assay and also on the number (and size) of labels to be detected. Nevertheless, it is our belief that once optimisation of MTJ sensors has been achieved, they will surpass the capability of SV sensors in bioassays, as was also the case for read head technology, and we should not forget that current commercial MTJ sensors employed in bioassays were not designed to work in a biological environment.

4.3 Magnetoimpedance biosensors

Another approach has been followed by workers such as Kurlyandskaya et al. [85–87], in which the giant magnetoimpedance (GMI) effect in Co-based amorphous nanowires is used to detect the presence of magnetic beads [26]. Such nanowires exhibit a circumferentially magnetised outer core, which is closely related to the magnetic field produced by a high-frequency AC current travelling along the wire. DC magnetic fields modify the circumferential magnetic permeability, which in turn alters the penetration depth of the AC current, which finally affects the impedance (at a given frequency). GMI sensors therefore detect the perturbations of the impedance due to stray fields produced by functionalised magnetic beads binding to the wire. Sensitivities of GMI sensors can be very high; for example, the GMI response of CoFeSiB-alloy nanowires around 15 μm in diameter can reach 40–100% per Oe [100]. However, the range of sensitivity can be limited; the GMI response falls off quickly with magnetic field, but improved alloys and fabrication techniques have resulted in nanowires which show over 100% GMI over a range of ±50–80 Oe [20].

GMI biosensors have been used to detect thin ferrofluid layers [87], magnetic microbeads [26, 86] and also Fe_3O_4 nanoparticles taken up (in large numbers) by human cells [20, 84]. However, as GMI is dependent on the effective skin depth, it is also sensitive to surface modification of the nanowires. A GMI biosensor could potentially detect not just biomolecules bound to magnetic labels, but also the binding of the biomolecules in a label-free manner [85, 88], via surface morphology or anisotropy changes caused by their presence.

4.4 Fluxgate biosensors

Some groups have designed magnetic bead biosensors based around the operation of the residence-time-difference (RTD) fluxgate magnetometer [2, 3, 114, 141], which consists of a current-carrying primary coil and a secondary pick-up coil, both wound around a ferromagnetic core. The AC current generates an oscillating magnetic field, which drives the core between its two stable saturated states and produces a periodic series of voltage spikes in the inductively coupled pick-up coil. The time intervals between a given spike and those before and after it are known as the residence times, which represent the times spent by the core in the two saturated states, and are normally equal. In the presence of a perturbing (usually DC) field, such as the dipole fields from magnetised beads, the residence times differ by an amount directly correlated to the perturbation. Due to the large number of micron-sized beads (min. 10^3) [3] required to give a detectable signal, these kind of sensors have only been demonstrated so far for mass-coverage assays or large encoded particles.

4.5 Biosensors combined with microfluidics

The experiments described above have been performed either in static liquid, by pipetting beads onto the sensors and allowing them to settle, or by transporting reagents and magnetic markers (micro- and nanobeads) to the sensors in microfluidic flow and allowing them to chemically bind. In a real lab-on-a-chip application, minimised user intervention and the requirements of high throughput naturally suggest the integration of microfluidic channels and bead sensors in a format which avoids the need for immobilisation of the beads to perform the detection. Nevertheless, to date few groups have attempted the fabrication challenge of integrating MR bead sensors into microfluidics [73, 134, 153] . Notable among those who successfully detected magnetic objects in flow are Pekas et al., who sensed ferrofluid plugs flowing in an oil-filled channel using GMR sensors in a Wheatstone bridge (Fig. 10). Using a commercial MTJ sensor (a 2 × 6 μm ellipse) within a 600 μm wide channel, Shen et al. were able to sense single 2.8 μm diameter M-280 Dynabeads® using an AC bridge configuration and two orthogonal in-plane DC fields.

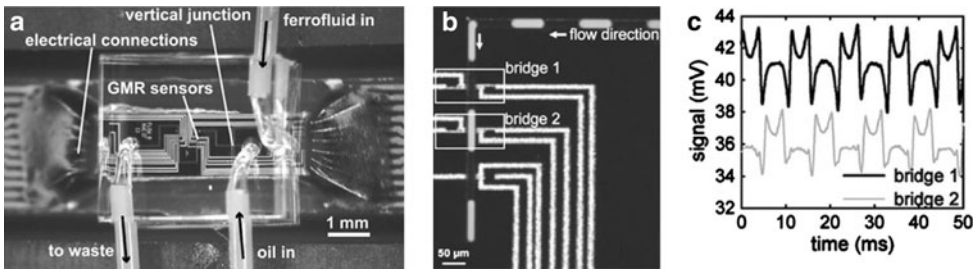

Fig. 10 **a** GMR sensors arranged in Wheatstone bridges integrated into microfluidics. **b** Composite optical and fluorescence micrograph showing plugs of ferrofluid in oil travelling over the sensors and **c** corresponding response of GMR sensor bridges. Reprinted from [134]

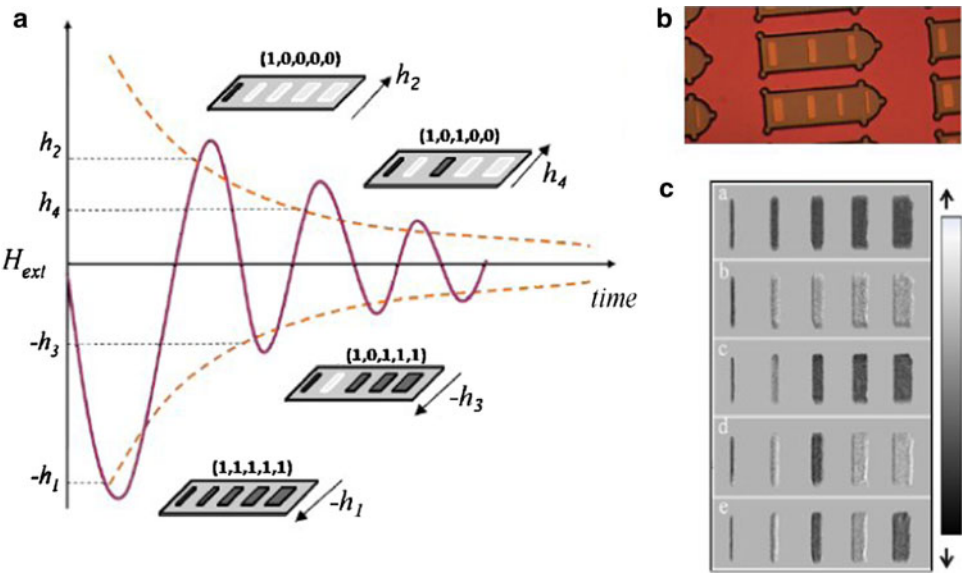

Fig. 11 **a** A schematic showing the multi-coercivity encoding scheme: a monotonically decreasing external magnetic field is applied to the entire microcarrier, writing each bit in turn, from hardest to softest. **b** Optical microscope image of three-bit and four-bit microcarriers, encapsulated in SU8 polymer. **c** A series of magneto-optical Kerr effect microscopy images showing the realisation of the scheme depicted in (**a**)

4.5.1 Magnetic signature-based bioassays

Our group is working on a library of magnetically encoded microcarriers that can be encoded and read within microfluidic channels (a detailed description of the protocol can be found in Ref. [68]). We aim to offer a high-throughput lab-on-a-chip multiplexing alternative to microarray technology, with initial applications aimed at point-of-care diagnostics. The design incorporates a row of coercivity-tuned thin film magnetic elements encapsulated in a biocompatible epoxy polymer (Fig. 11). The magnetic shape anisotropy is used to control the critical applied magnetic field required to switch the magnetisation of an element between its two stable states, thus creating a binary barcode. The key advantages of this type of strategy are: (i) the number of unique signatures doubles with each additional magnetic bit providing an incredible scalability; (ii) the microcarriers are identical prior to encoding/functionalisation so that they can be mass produced cost effectively; (iii) in-flow (re-)write ability allows reaction tracking, ideal for combinatorial chemistry applications; (iv) a digital electronic readout from the magnetoresistive sensor removes the constraints of an optical measurement for encoding and analyte binding identification [114].

5 Summary

In conclusion, we have discussed sequencing methods such as '454' and four-colour sequencing. These established methods are massively parallel, fast and accurate, but are only really useful for DNA sequencing. Even though the read-out time is short, the amplification steps required for the sample is time consuming. For biomolecular recognition of non-DNA targets such as proteins in biological fluids, a more widely encountered problem in clinical diagnostics, alternative assays have been developed which similarly to sequencing techniques rely on optical labelling. Whereas sequencing methods only need to distinguish the four bases, these assays must uniquely identify a much larger panel of biologically relevant molecules. Designers of labels for optical encoding and detection methods have concentrated mainly on fluorescent labels such as QDs and fluorophores and on graphically encoded labels such as nanowire barcodes. However, fluorescent bioassays suffer from bleaching, autofluorescence and spectral overlap, whereas graphical labels must be imaged, with the associated disadvantages of non-real time analysis and non-miniaturisable detection set-ups known from microarray methods. The problems associated with optical labelling

have inspired the efforts of several research groups to develop a complete magnetic bioassay platform based on functionalised magnetic particles and magnetic sensors, which do not suffer from the same constraints. Furthermore, magnetic labelling of biomolecules is particularly attractive as there is no magnetic background in the vast majority of biological samples. However, we pointed out that implementation of magnetic labels require biocompatibility, monodispersity and correct functionalisation to reduce non-specific binding.

The current sizes of the magnetic beads used as labels for the various biomedical applications vary from a few micrometers to tens of nanometers for in vitro biosensing, whereas for in vivo applications such as MRI contrast agents they are only a few nanometers in size. For magnetic biosensors the trend seems to go towards ever smaller sizes, but for quantitative measurements of the total magnetic moment of the detected beads (for example for mass-coverage sensor) the size and the magnetic moment distributions of the nanoparticles present a limiting factor at present. Micron-sized particles usually comprise a large number of magnetic nanoparticles in a silica or polymer matrix, which permits better control over the total magnetic moment during fabrication and moment selective sorting post fabrication. However, as better protocols for synthesising magnetic nanoparticles are developed, applications which favour particles of a few tens of nanometers or below will benefit from the improvement in size and moment distributions. The optimal size of a nanoparticle depends also on the physical properties required for a specific application; whether they need to be superparamagnetic, to avoid agglomeration or excessive heat dissipation for MRI and hyperthermia applications, or ferromagnetic, to maintain a remanent magnetisation for quantitative biosensing measurements. With respect to the different magnetic biosensor types different authors choose particle sizes suitable for their requirements such as the sensitivity of their detection system.

A variety of magnetic sensors have been employed as detectors for magnetic labels. Despite their different principles of operation, two avenues have been explored, with some success: mass-coverage sensors with active areas of hundreds of square microns which provide statistical counting of a large number of magnetic labels, and micron-sized sensors aimed at detecting the presence of single micro- or nano-beads. Although single-bead detection has already been demonstrated by Hall crosses and MR sensors both in static flow and in microfluidics, and significant progress has been made with mass-coverage sensors towards an actual bioassay, a complete multiplexed bioassay has not yet been demonstrated to our knowledge. The main obstacles to this goal seem to be integration of the sensors with microfluidics to efficiently transport beads and reagent and the design of some method of controlling the position of the beads to maximise the signal (particularly important for smaller magnetic particles).

Nevertheless, advances have been made towards the goal of a complete multiplexed bioassay. In particular, comparative studies [52, 151] between contemporary fluorescent assays and their magnetic counterparts indicate that magnetic sensors have an improved sensitivity over a much larger analyte concentration range from atto- to nanomolar, inaccessible to fluorescent techniques such as ELISA. Statistical errors in the magnetic response are currently slightly larger, but quantitative detection comparisons agree to within 9% at the ng/ml level. Other advantages gained from the magnetic sensors include real-time monitoring of analyte level and reduced amplification stages of the analytes of interest with the possibility of removing amplification altogether, if the signal-to-noise levels can be improved.

Given the wide range of sensor designs which have been successfully used to detect magnetic labels, the question naturally arises of which kinds of sensors might be most appropriate to measure labels lying in a particular size range. From the reports reviewed above, most groups rely on magnetoresistance or Hall effect based sensors, despite the existence of fluxgate and even SQUID–based sensors [24], which do not seem to confer a major advantage over the former relative to the greater difficulty of implementation. MR based sensors are the most popular choice for mass-coverage detection and a move towards TMR array sensors is foreseeable. Nevertheless, it seems that Hall sensors may be best suited to detect labels of dimension 50 nm and below, due to their simple single-layer construction and relatively high signal-to-noise ratio, as this simplifies the fabrication of sensors of similar size to the labels detected. Hall sensors with a 40×40 nm active area have been fabricated in Bi thin films at the apex of an AFM tip [31, 136] using focused-ion beam milling. However, the oft-quoted requirement to size-match sensor and label (to maximise the intensity of the magnetic field intercepted by the sensor) has been challenged by a new design by Vavassori et al. [167] based on AMR. When a dilute solution of magnetic particles of diameter 130 nm was dispensed onto a square Py ring, they were attracted to the corners of the ring which contained domain walls.[9] As the domain walls are highly localised magnetisation perturbations, which interacted strongly with the magnetic nanoparticles, measurements of the AMR of the ring revealed an increase of 12 ± 2 Oe in the external applied field required to displace the domain wall, similar to the bead detection

[9] Domain walls are the transitional regions between areas of different magnetisation orientation.

scheme used in [98]. A further point of note is that by using the the domain wall's own magnetic field to draw the particles out of solution and localise them, avoided the need for further external means of positioning the nanoparticles precisely with respect to the sensor, which has always been necessary for any single-bead sensing bioassay regardless of the sensor type used.

So far, magnetic labels only encode one bit of information, which does not need to be the case as encoded microcarriers (magnetic barcodes) have been developed by our group for use in an integrated microfluidic bio-chip. The barcodes provide a mobile substrate for solution phase reactions and identify the biomolecules bound to their surfaces through an embedded multi-bit magnetic signature [68]. The combination of flow cytometry and encoded labels offers an advantage over hybridisation assays by providing multiplexed detection without the need to 'regenerate' the sensors. The scalability of this approach allows not only biological fluid interrogation for a panel of proteins at the same time, but can also challenge current DNA sequencing techniques by providing an unique code for each combination of a number of bases while maintaining the speed and accuracy of magnetic read-out.

We have shown that magnetic biosensing has the potential to replace or to complement existing fluorescence based in vitro biosensor techniques by facilitating detection, manipulation and sorting of analytes. However, 'cellular' in vivo magnetic biosensor applications, despite the existence of first attempts such as the magnetic actuation for control of cellular function [129] and detection of endogenously produced magnetic nanoparticles by a TMR sensor [72], remain a task for the future.

Acknowledgements We would like to thank the EPSRC for financial support.

References

1. Alizadeh AA et al (2000) Distinct types of diffuse large B-cell lymphoma identified by gene expression profiling. Nature 403:503–511
2. Andò B, Baglio S, Bulsara AR, Sacco V (2005) "Residence times difference" fluxgate magnetometers. IEEE Sens J 5(5):895–904
3. Andò B, Ascia A, Baglio S, Bulsara AR, In V, Pitrone N, Trigona C (2008) Residence times difference fluxgate magnetometer for magnetic biosensing. AIP Conf Proc 1025:139–149
4. Axelrod D, Burghardt TP, Thompson NL (1984) Total internal reflection fluorescence. Annu Rev Biophys Bioeng 13:247–268
5. Baibich MN, Broto JM, Fert A, Dau FNV, Petroff F (1988) Giant magnetoresistance of (001)Fe/(001)Cr magnetic superlattices. Phys Rev Lett 61:2472–2475
6. Bain CD, Whitesides GM (1989) Formation of monolayers by the coadsorption of thiols on gold: variation in the length of the alkyl chain. J Am Chem Soc 111(18):7164–7175
7. Bain CD, Biebuyck HA, Whitesides GM (1989) Comparison of self-assembled monolayers on gold: coadsorption of thiols and disulfides. Langmuir 5:723–727
8. Bain CD, Evall J, Whitesides GM (1989) Formation of monolayers by the coadsorption of thiols on gold: variation in the head group, tail group, and solvent. J Am Chem Soc 111(18):7155–7164
9. Bandyopadhyay K, Patil V, Vijayamohanan K, Sastry M (1997) Adsorption of silver colloidal particles through covalent linkage to self-assembled monolayers. Langmuir 13(20):5244–5248
10. Banu S, Birtwell S, Galitonov G, Chen Y, Zheludev N, Morgan H (2007) Fabrication of diffraction-encoded micro-particles using nano-imprint lithography. J Micromech Microeng 17: S116–S121
11. Baselt DR, Lee GU, Colton RJ (1996) Biosensor based on force microscope technology. J Vac Sci Technol B 14(2):789–793
12. Baselt DR, Lee GU, Natesan M, Metzger SW, Sheehan PE, Colton RJ (1998) A biosensor based on magnetoresistance technology. Biosens Bioelect 13:731–739
13. Bauer LA, Reich DH, Meyer GJ (2003) Selective functionalization of two-component magnetic nanowires. Langmuir 19:7043–7048
14. Bennett ST, Barnes C, Cox A, Davies L, Brown C (2005) Toward the $1000 human genome. Pharmacogenomics 6:373–382
15. Berggren C, Johansson G (1997) Capacitance measurements of antibody-antigen interactions in a flow system. Anal Chem 69(18):3651–3657
16. Berry CC (2009) Progress in functionalization of magnetic nanoparticles for applications in biomedicine. J Phys D 42: 224,003
17. Besse PA, Boero G, Demierre M, Pott V, Popovic R (2002) Detection of a single magnetic microbead using a miniaturized silicon Hall sensor. Appl Phys Lett 80:4199–4201
18. Bier F, Kleinjung F (2001) Feature-size limitations of microarray technology: a critical review. Fresen J Anal Chem 371: 151–156
19. Binasch G, Grünberg P, Saurenbach F, Zinn W (1989) Enhanced magnetoresistance in layered magnetic structures with antiferromagnetic interlayer exchange. Phys Rev B 39(7):4828–4830
20. Blanc-Beguin F, Nabily S, Gieraltowski J, Turzo A, Querellou S, Salaun PY (2009) Cytotoxicity and GMI bio-sensor detection of maghemite nanoparticles internalized into cells. J Magn Magn Mater. 321:192–197
21. Braeckmans K, Smedt SCD, Roelant C, Leblans M, Pauwels R, Demeester J (2003) Encoding microcarriers by spatial selective photobleaching. Nat Mater 2:169–173
22. Brzeska M, Panhorst M, Kamp PB, Schotter J, Reiss G, Pühler A, Becker A, Brückl H (2004) Detection and manipulation of biomolecules by magnetic carriers. J Biotechnol 112:25–33
23. Cao YWC, Jin RC, Mirkin CA (2002) Nanoparticles with Raman spectroscopic fingerprints for DNA and RNA detection. Science 297:1536–1540
24. Carr C, Matlachov AN, Sandin H, Espy MA, Kraus RH (2007) Magnetic sensors for Bioassay: HTS SQUIDs or GMRs? IEEE Trans Appl Supercon 17:808–811
25. Cavalli G, Banu S, Ranasinghe T, Broder GR, Martins HFP, Neylon C, Morgan H, Bradley M, Roach PL (2007) Multistep synthesis on SU-8: combining microfabrication and solid-phase chemistry on a single material. J Combin Chem 9(3):462–472
26. Chiriac H, Tibu M, Moga AE, Herea DD (2005) Magnetic GMI sensor for detection of biomolecules. J Magn Magn Mater 293:671–676
27. Choi JW, Oh KW, Thomas JH, Heineman WR, Halsall HB, Nevin JH, Helmicki AJ, Henderson HT, Ahn CH (2002) An integrated microfluidic biochemical detection system for protein

analysis with magnetic bead-based sampling capabilities. Lab Chip 2:27–30
28. Chu S, DeRisi J, Eisen M, Mulholland J, Botstein D, Brown PO, Herskowitz I (1998) The transcriptional program of sporulation in budding yeast. Science 282:699–705
29. Chung SH, Hoffmann A, Bader SD, Liu C, Kay B, Makowski L, Chen L (2004) Biological sensors based on Brownian relaxation of magnetic nanoparticles. Appl Phys Lett 85(14):2971–2973
30. Cleary MA et al (2004) Production of complex nucleic acid libraries using highly parallel in situ oligonucleotide synthesis. Nat Meth 1:241–248
31. Cowburn RP, Jausovec AV, Petit D (2009) Nanoscale Magnetic Field Sensors for Biological Applications. Talk given at Biomagnetic Sensing Workshop, Cambridge, UK
32. Dieny B, Speriosu VS, Gurney BA, Parkin SSP, Wilhoit DR, Roche KP, Metin S, Peterson DT, Nadimi S (1991) Spin-valve effect in soft ferromagnetic sandwiches. J Magn Magn Mater 93:101–104
33. Dressman D, Yan H, Traverso G, Kinzler KW, Vogelstein B (2003) Transforming single DNA molecules into fluorescent magnetic particles for detection and enumeration of genetic variations. Proc Natl Acad Sci USA 100:8817–8822
34. Eastman PS, Ruan W, Doctolero M, Nuttall R, de Feo G, Park JS, Chu JSF, Cooke P, Gray JW, Li S, Chen FF (2006) Qdot nanobarcodes for multiplexed gene expression analysis. Nano Lett 6(5):1059–1064
35. Ejsing L, Hansen MF, Menon AK, Ferreira HA, Graham DL, Freitas PP (2004) Planar Hall effect sensor for magnetic micro- and nanobead detection. Appl Phys Lett 84(23):4729–4731
36. Ejsing L, Hansen MF, Menon AK, Ferreira HA, Graham DL, Freitas PP (2005) Magnetic microbead detection using the planar Hall effect. J Magn Magn Mater 293(1):677–684
37. Ekins R, Chu FW (1999) Microarrays: their origins and applications. Trends Biotechnol 17:217–218
38. Erdem A, Pividori MI, Lermo A, Bonanni A, del Valle M, Alegret S (2006) Genomagnetic assay based on label-free electrochemical detection using magneto-composite electrodes. Sens Actuators B 114:591–598
39. Erickson D, Li D (2004) Integrated microfluidic devices (review). Anal Chim Acta 507:11–26
40. Estrela P, Stewart AG, Yan F, Migliorato P (2005) Field effect detection of biomolecular interactions. Electrochim Acta 50(25–26):4995–5000
41. Evans M, Sewter C, Hill E (2003) An encoded particle array tool for multiplex bioassays. Assay Drug Dev Technol 1:199–207
42. Fan JB, Chee MS, Gunderson KL (2006) Highly parallel genomic assays. Nat Rev Genet 7:632–644
43. Ferreira H, Graham D, Feliciano N, Clarke L, Amaral M, Freitas PP (2005) Detection of cystic fibrosis related DNA targets using AC field focusing of magnetic labels and spin-valve sensors. IEEE Trans Magn 41(10):4140–4142
44. Ferreira HA, Cardoso FA, Ferreira R, Cardoso S, Freitas PP (2006) Magnetoresistive DNA chips based on ac field focusing of magnetic labels. J Appl Phys 99:08P105
45. Fodor SP et al (1991) Light-directed, spatially addressable parallel chemical synthesis. Science 251:767–773
46. Fraser CM et al (1995) The minimal gene component of *Mycoplasma genitalium*. Science 270:397–403
47. Frederix F, Bonroy K, Laureyn W, Reekmans G, Campitelli A, Dehaen W, Maes G (2003) Enhanced performance of an affinity biosensor interface based on mixed self-assembled monolayers of thiols on gold. Langmuir 19(10):4531–4537
48. Freitas PP, Ferreira HA, Graham DL, Clarke L, Amaral M, Martins V, Fonseca L, Cabral JS (2004) Magnetoresistive biochips. Europhys News 36(6):224–226
49. Freitas PP, Ferreira R, Cardoso S, Cardoso F (2007) Magnetoresistive sensors. J Phys Condens Matter 19:165,221
50. Galitonov G, Birtwell S, Zheludev N, Morgan H (2006) High capacity tagging using nanostructured diffraction barcodes. Opt Express 14:1382–1387
51. Gallagher WJ, Parkin SSP (2006) Development of the magnetic tunnel junction MRAM at IBM: from first junctions to a 16-Mb MRAM demonstrator chip. IBM J Res Dev 50:5–23A
52. Gaster RS, Hall DA, Nielsen CH, Osterfeld SJ, Yu H, Mach KE, Wilson RJ, Murmann B, Liao JC, Gambhir SS, Wang SX (2009) Matrix-insensitive protein assays push the limits of biosensors in medicine. Nat Med 15:1327–1332
53. Gehanno V, Freitas PP, Veloso A, Ferreira J, Almeida B, Sousa JB, Kling A, Soares JC, da Silva MF (1999) Ion beam deposition of Mn-Ir spin valves. IEEE Trans Magn 35(5):4361–4367
54. Goloverda G, Jackson B, Kidd C, Kolesnichenko V (2009) Synthesis of ultrasmall magnetic iron oxide nanoparticles and study of the colloid and surface chemistry. J Magn Magn Mater 321:1372–1376
55. Golub TR, Slonim DK, Tamayo P, Huard C, Gaasenbeek M, Mesirov JP, Coller H, Loh ML, Downing JR, Caligiuri MA, Bloomfield CD, Lander ES (1999) Molecular classification of cancer: class discovery and class prediction by gene expression monitoring. Science 286:531–537
56. Graham DL, Ferreira HA, Bernardo J, Freitas PP, Cabral JMS (2003) Single magnetic microsphere placement and detection on-chip using current line designs with integrated spin valve sensors: biotechnological applications. J Appl Phys 91(10): 7786–7788
57. Graham D, Ferreira H, Freitas P, Cabral J (2003) High sensitivity detection of molecular recognition using magnetically labelled biomolecules and magnetoresistive sensors. Biosens Bioelect 18:483–488
58. Graham DL, Ferreira HA, Freitas PP (2004) Magnetoresistive-based biosensors and biochips (review). Trends Biotechnol 22(9):455–462
59. Graham D, Ferreira H, Feliciano N, Freitas PP, Clarke L, Amaral M (2005) Magnetic field-assisted DNA hybridisation and simultaneous detection using micron-sized spin-valve sensors and magnetic nanoparticles. Sens Actuators B 107:936–944
60. Grancharov SG, Zeng H, Sun S, Wang SX, O'Brien S, Murray CB, Kirtley JR, Held GA (2005) Bio-functionalization of monodisperse magnetic nanoparticles and their use as biomolecular labels in a magnetic tunnel junction based sensor. J Phys Chem B 109:13,030–13,035
61. Hall ED (1879) On a new action of the magnet on electric currents. Am J Math 2:287–292
62. Han M, Gao X, Su JZ, Nie S (2001) Quantum dot tagged microbeads for multiplexed optical coding of biomolecules. Nat Biotechnol 19:631–635
63. Harder P, Grunze M, Dahint R, Whitesides GM, Laibinis PE (1998) Molecular conformation in oligo(ethylene glycol)-terminated self-assembled monolayers on gold and silver surfaces determines their ability to resist protein adsorption. J Phys Chem B 102:426–436
64. Hayward TJ, Llandro J, Kopper KP, Trypiniotis T, Mitrelias T, Bland JAC, Barnes CHW (2008) Towards magnetic suspension assay technology. AIP Conf Proc 1025:111–124
65. Hermanson GT (1996) Bioconjugate techniques. Academic Press, San Diego, CA
66. Hickman JJ, Laibinis PE, Auerbach DI, Zou C, Gardner TJ, Whitesides GM, Wrighton MS (1992) Toward orthogonal self-assembly of redox active molecules on Pt and Au: selective reaction of disulfide with Au and isocyanide with Pt. Langmuir 8:357–359

67. Hong J, Noma K, Kanda E, Kanai H (2003) Very large giant magnetoresistance of spin-valves with specularly reflective oxide layers. Appl Phys Lett 83(5):960–962
68. Hong B, Jeong JR, Llandro J, Hayward TJ, Ionescu A, Trypiniotis T, Mitrelias T, Kopper KP, Steinmuller SJ, Bland JAC (2008) High throughput biological analysis using multi-bit magnetic digital planar tags. AIP Conf Proc 1025:74–81
69. Hughes TR et al (2001) Expression profiling using microarrays fabricated by an ink-jet oligonucleotide synthesizer. Nat Biotechnol 19:342–347
70. Iler RK (1979) The chemistry of silica. Wiley, New York
71. Ilic B, Craighead H, Krylov S, Senaratne W, Ober C, Neuzil P (2004) Attogram detection using nanoelectromechanical oscillators. J Appl Phys 95(7):3694–3703
72. Ionescu A, Darton NJ, Vyas KN, Llandro J (2010) Detection of endogenous magnetic nanoparticles with a TMR sensor. Philos Trans R Soc A. doi:10.1098/rsta.2010.0137
73. Jiang Z, Llandro J, Mitrelias T, Bland JAC (2006) An integrated microfluidic cell for detection, manipulation, and sorting of single micron-sized magnetic beads. J Appl Phys 99:08S105
74. Jordan A, Scholz R, Wust P, Fahling H, Felix R (1999) Magnetic fluid hyperthermia (MFH): Cancer treatment with AC magnetic field induced excitation of biocompatible superparamagnetic nanoparticles. J Magn Magn Mater 201(1):413–419
75. Joshi M, Pinto R, Rao VR, Mukherji S (2007) Silanization and antibody immobilization on SU-8. Appl Surf Sci 253:3127–3132
76. Ju J, Kim DH, Bi L, Meng Q, Bai X, Li Z, Li X, Marma MS, Shi S, Wu J, Edwards JR, Romu A, Turro NJ (2006) Four-color DNA sequencing by synthesis using cleavable fluorescent nucleotide reversible terminators. Proc Natl Acad Sci USA 103:19,635–19,640
77. Julliere M (1975) Tunnelling between ferromagnetic films. Phys Lett A 54A(3):225–226
78. Karpovich DS, Blanchard GJ (1996) Dynamics of a tethered chromophore imbedded in a self-assembled monolayer. Langmuir 12:5533–5524
79. Kastl KF, Lowe CR, Norman CE (2008) Encoded and multiplexed surface plasmon resonance sensor platform. Anal Chem 80:7862–7869
80. Kausaite A, van Dijk M, Castrop J, Ramanaviciene A, Baltrus JP, Acaite J, Ramanavicius A (2007) Surface plasmon resonance label-free monitoring of antibody antigen interactions in real time. Biochem Mol Biol Educ 5(1):57–63
81. Kriz CB, Rådevik K, Kriz D (1996) Magnetic permeability measurements in bioanalysis and biosensors. Anal Chem 68(11):1966–1970
82. Kuijk K, van Gestel W, Gorter F (1975) The barber pole, a linear magnetoresistive head. IEEE Trans Magn 11(5):1215–1217
83. Kumagai Y, Imai Y, Abe M, Sakamoto S, Handa H, Sandhu A (2008) Sensitivity dependence of Hall biosensor arrays with the position of superparamagnetic beads on their active regions. J Appl Phys 103:07A309
84. Kumar A, Mohapatra S, Miyar VF, Cerdeira A, Garcia JA, Srikanth H, Gass J, Kurlyandskaya GV (2007) Magnetoimpedance biosensor for Fe_3O_4 nanoparticle intracellular uptake evaluation. Appl Phys Lett 91:143,902
85. Kurlyandskaya G (2009) Giant magnetoimpedance for biosensing: advantages and shortcomings. J Magn Magn Mater 321:659–662
86. Kurlyandskaya G, Levit V (2005) Magnetic Dynabeads® detection by sensitive element based on giant magnetoimpedance. Biosens Bioelect 20:1611–1616
87. Kurlyandskaya GV, Sanchez ML, Hernando B, Prida VM, Gorria P, Tejedor M (2003) Giant-magnetoimpedance-based sensitive element as a model for biosensors. Appl Phys Lett 82:3053–3055
88. Kurlyandskaya GV, Miyar VF, Saad A, Asua E, Rodriguez J (2007) Giant magnetoimpedance: A label-free option for surface effect monitoring. J Appl Phys 101:054,505
89. Kyo M, Usui-Aoki K, Koga H (2005) Label-free detection of proteins in crude cell lysate with antibody arrays by a surface plasmon resonance imaging technique. Anal Chem 77(22): 7715–7121
90. Lagae L, Wirix-Speetjens R, Das J, Graham DL, Ferreira HA, Freitas PP, Borghs G, Boeck JD (2002) On-chip manipulation and magnetization assessment of magnetic bead ensembles by integrated spin-valve sensors. J Appl Phys 91(10):7445–7447
91. Lahiri J, Assacs L, Tien J, Whitesides GM (1999) A strategy for the generation of surfaces presenting ligands for studies of binding based on an active ester as a common reactive intermediate: a surface plasmon resonance study. Anal Chem 71(4): 777–790
92. Laibinis PE, Hickman JJ, Wrighton MS, Whitesides GM (1989) Orthogonal self-assembled monolayers: alkanethiols on gold and alkane carboxylic acids on alumina. Science 245:845–847
93. Lany M, Boero G, Popovic RS (2005) Superparamagnetic microbead inductive detector. Rev Sci Instrum 76:084,301
94. Lee SY, Harris MT (2006) Surface modification of magnetic nanoparticles capped by oleic acids: characterization and colloidal stability in polar solvents. J Colloid Interface Sci 293: 401–408
95. Li G, Wang SX (2004) Model and experiment of detecting multiple magnetic nanoparticles as biomolecular labels by spin valve sensors. IEEE Trans Magn 40:3000–3002
96. Li G, Joshi V, White RL, Wang SX, Kemp JT, Webb C, Davis RW, Sun S (2003) Detection of single micron-sized magnetic bead and magnetic nanoparticles using spin valve sensors for biological applications. J Appl Phys 93(10):7557–7559
97. Li G, Sun S, Wilson RJ, White RL, Pourmand N, Wang SX (2006) Spin-valve sensors for ultrasensitive detection of superparamagnetic nanoparticles for biological applications. Sens Actuators A 126:98–106
98. Llandro J, Hayward TJ, Morecroft D, Bland JAC, Castaño FJ, Colin IA, Ross CA (2007) Quantitative digital detection of magnetic beads using pseudo-spin-valve rings for multiplexed bioassays. Appl Phys Lett 91:203,904
99. Love JC, Estroff LA, Kriebel JK, Nuzzo RG, Whitesides GM (2005) Self-assembled monolayers of thiolates on metals as a form of nanotechnolgy. Chem Rev 105(4):1103–1169
100. Mahdi AE, Panina L, Mapps D (2003) Some new horizons in magnetic sensing: high-Tc SQUIDs, GMR and GMI materials. Sens Actuators A 105:271–285
101. Maoz R, Cohen H, Sagiv J (1998) Specific nonthermal chemical structural transormation induced by microwaves in a single amphiphilic bilayer self-assembled on silicon. Langmuir 14:5988–5993
102. Margulies M et al (2005) Genome sequencing in microfabricated high-density picolitre reactors. Nature 437:376–380
103. Marie R, Schmid S, Johansson A, Ejsing L, Mordstrom M, Hafliger D, Christensen CBV, Boisen A, Dufva M (2006) Immobilisation of DNA to polymerised SU-8 photoresist. Biosens Bioelectron 21(7):1327–1332
104. Martin BR, Dermody DJ, Reiss BD, Fang M, Lyon LA, Natan MJ, Mallouk TE (1999) Orthogonal self-assembly on colloidal gold-platinum nanorods. Adv Mater 11:1021–1025
105. Martins VC, Cardoso FA, Loureiro J, Mercier M, Germano J, Cardoso S, Ferreira R, Fonseca LP, Sousa L, Piedade MS, Freitas PP (2008) Integrated spintronic platforms for biomolecular recognition detection. AIP Conf Proc 1025:150–175
106. Massart R, Cabuil V (1987) Synthesis of colloidal magnetite in alkaline medium: yield and particle size control. J Chim Phys 84:967–973

107. Mbindyo JKN, Reiss BD, Martin BR, Keating CD, Natan MJ, Mallouk TE (2001) DNA-directed assembly of gold nanowires on complementary surfaces. Adv Mater 13:249–254
108. Medintz IL, Uyeda HT, Goldman ER, Mattoussi H (2005) Quantum dot bioconjugates for imaging, labelling and sensing. Nat Mater 4:435–446
109. Megens M, Prins M (2005) Magnetic biochips: a new option for sensitive diagnostics. J Magn Magn Mater 293:702–708
110. Mihajlović G, Xiong P, von Molnár S, Ohtani K, Ohno H, Field M, Sullivan GJ (2005) Detection of single magnetic bead for biological applications using an InAs quantum-well micro-Hall sensor. Appl Phys Lett 87:112,502
111. Miller MM, Sheehan PE, Edelstein RL, Tamanaha CR, Zhong L, Bounnak S, Whitman LJ, Colton RJ (2001) A DNA array sensor utilizing magnetic microbeads and magnetoelectronic detection. J Magn Magn Mater 225(5):138–144
112. Miller MM, Prinz GA, Cheng SF, Bounnak S (2002) Detection of a micron-sized magnetic sphere using a ring-shaped anisotropic magnetoresistance-based sensor: a model for a magnetoresistance-based biosensor. Appl Phys Lett 81(12):2211–2213
113. Mitra RD, Church GM (1999) In situ localized amplification and contact replication of many individual DNA molecules. Nucleic Acids Res 27:e34
114. Mitrelias T, Trypiniotis T, van Belle F, Kopper KP, Steinmuller SJ, Bland JAC, Robertson PA (2008) Magnetic microtags and magnetic encoding for applications in biotechnology. AIP Conf Proc 1025:60–73
115. Molday RS, Mackenzie D (1982) Immunospecific ferromagnetic iron-dextran reagents for the labeling and magnetic separation of cells. J Immunol Methods 52(3):353–367
116. Moodera JS, Kinder LR, Wong TM, Meservey R (1995) Large magnetoresistance at room temperature in ferromagnetic thin-film tunnel junctions. Phys Rev Lett 74:3273–3276
117. Motesharei K, Myles DC (1998) Molecular recognition on functionalised self-assembled monolayers of alkanethiols on gold. J Am Chem Soc 120:7328–7336
118. Mullis K, Faloona F, Sharf S, Saiki R, Horn G, Erlich H (1986) Specific enzymatic amplification of DNA in vitro—the polymerase chain-reaction. Cold Spring Harb Symp Quant Biol 51(1):263–273
119. Mulvaney SP, Mattoussi HM, Whitman LJ (2004) Incorporating fluorescent dyes and quantum dots into magnetic microbeads for immunoassays. Biotechniques 36(4):602–609
120. Nicewarner-Peña SR, Freeman RG, Reiss BD, He L, Peña DJ, Walton ID, Cromer R, Keating CD, Natan MJ (2001) Submicrometer metallic barcodes. Science 294:137–141
121. Nicewarner-Peña SR, Freeman RG, Reiss BD, He L, Pena DJ, Walton ID, Cromer R, Keating C, Natan M (2001) Submicrometer metallic barcodes. Science 294:137–141
122. Nuzzo RG, Zegarski BR, Dubois LH (1987) Fundamental studies of the chemisorption of organosulfur compounds on Au(111). Implications for molecular self-assembly on gold surfaces. J Am Chem Soc 109:733–740
123. Nyren P (1987) Enzymatic method for continuous monitoring of DNA polymerase activity. Anal Biochem 167:235–238
124. Onclin S, Ravoo BJ, Reinhoudt DN (2005) Engineering silicon oxide surfaces using self-assembled monolayers. Angew Chem Int Ed 44:6282–6304
125. Osbourne MA, Furey WS, Klenerman D, Balasubramanian S (2000) Single molecule analysis of DNA immobilised on microspheres. Anal Chem 72:3678–3681
126. Palfreyman JJ (2008) Fabrication and functionalisation of multibit magnetic tags. Ph.D. thesis, University of Cambridge
127. Palfreyman JJ, van Belle F, Lew WS, Mitrelias T, Bland JAC, Lopalco M, Bradley M (2007) Hybridization of electrodeposited magnetic multilayer micropillars. IEEE Trans Magn 43(6):2439
128. Palma RD, Laureyn W, Frederix F, Bonroy K, Pireaux JJ, Borghs G, Maes G (2007) Formation of dense self-assembled monolayers of (n-decyl)trichlorosilanes on Ta/Ta_2O_5. Langmuir 23(2):443–451
129. Pankhurst QA, Thanh NKT, Jones SK, Dobson J (2009) Progress in application of magnetic nanoparticles in biomedicine. J Phys D 42:224,001
130. Park SJ, Taton TA, Mirkin CA (2002) Array-based electrical detection of DNA with nanoparticle probes. Science 295:1503–1506
131. Parkin SSP (1998) The magic of magnetic multilayers. IBM J Res Dev 42(1):3–6
132. Patel N, Davies MC, Heaton RJ, Roberts CJ, Tendler SJB, Williams PM (1998) A scanning probe microscopy study of the physisorption and chemisorption of protein molecules onto carboxylate terminated self-assembled monolayers. Appl Phys A 66:569–574
133. Peck W (2007) DNA microarray technology—engineering, manufacture, and applications. LSSU Genomics, Agilent Technologies, Inc. Talk given at University of Cambridge Computing Laboratory
134. Pekas N, Porter MD, Tondra M, Popple A, Jander A (2004) Giant magnetoresistance monitoring of magnetic picodroplets in an integrated microfluidic system. Appl Phys Lett 85(20):4783–4785
135. Peterson AW, Heaton RJ, Georgiadis RM (2001) The effect of surface probe desnisty on DNA hybridisation. Nucleic Acids Res 29(24):5163–5168
136. Petit D, Faulkner CC, Johnstone S, Wood D, Cowburn RP (2005) Nanometer scale patterning using focused ion beam milling. Rev Sci Instrum 76:026,105
137. Pregibon DC, Toner M, Doyle PS (2007) Multifunctional encoded particles for high-throughput biomolecule analysis. Science 315:1393–1396
138. Reich DH, Tanase M, Hultgren A, Bauer LA, Chen CS, Meyer GJ (2003) Biological applications of multifunctional magnetic nanowires (invited). J Appl Phys 93:7275–7280
139. Reiss G, Brückl H, Hütten A, Schotter J, Brzeska M, Panhorst M, Sudfeld D, Becker A, Kamp PB, Pühler A, Wojczykowski K, Jutzi P (2005) Magnetoresistive sensors and magnetic nanoparticles for biotechnology. J Mater Res 20(12):3294–3304
140. Rife JC, Miller MM, Sheehan PE, Tamanaha CR, Tondra M, Whitman LJ (2003) Design/performance of GMR sensors for detection of magnetic microbeads. Sens Actuators A 107(3):209–218
141. Ripka P (2003) Advances in fluxgate sensors. Sens Actuators A 106:8–14
142. Roca AG, Costo R, Rebolledo AF, Veintemillas-Verdaguer S, Tartaj P, Gonzalez-Carreno T, Morales MP, Serna CJ (2009) Progress in the preparation of magnetic nanoparticles for applications in biomedicine. J Phys D 42:224,002
143. Ronaghi M, Karamohamed S, Petterson B, Uhlin M, Nyren P (1996) Real-time DNA sequencing using detection of pyrophosphate release. Anal Biochem 242:84–89
144. Salem AK, Searson PC, Leong KW (2003) Multifunctional nanorods for gene delivery. Nat Mater 2:668–671
145. Sandhu A, Handa H (2005) Practical Hall sensors for biomedical instrumentation. IEEE Trans Magn 41:4123–4127
146. Sandhu A, Sanbonsugi H, Shibasaki I, Abe M, Handa H (2004) High sensitivity InSb ultra-thin film micro-Hall sensors for bioscreening applications. Jpn J Appl Phys 43:868–870
147. Sanger F, Coulsen AR (1975) A rapid method for determining sequences in DNA by primed synthesis with DNA polymerase. J Mol Biol 94:441–448
148. Sanger F, Nicklen S, Coulsen AR (1977) DNA sequencing with chain-terminating inhibitors. Proc Natl Acad Sci USA 74:5463–5467

149. Schena M, Shalon D, Davis R, Brown P (1995) Quantitative monitoring of gene expression patterns with a complementary DNA microarray. Science 270:467–470
150. Schotter J, Kamp PB, Becker A, Pühler A, Brinkmann D, Schepper W, Brückl H, Reiss G (2002) A biochip based on magnetoresistive sensors. IEEE Trans Magn 38(5):3365–3367
151. Schotter J, Kamp PB, Becker A, Pühler A, Reiss G, Brückl H (2004) Comparison of a prototype magnetoresistive biosensor to standard fluorescent DNA detection. Biosens Bioelect 19:1149–1156
152. Seino S, Kinoshita T, Nakagawa T, Kojima T, Taniguci R, Okuda S, Yamamoto TA (2008) Radiation induced synthesis of gold/iron-oxide composite nanoparticles using high-energy electron beam. J Nanoparticle Res 10(6):1071–1076
153. Shen W, Liu X, Mazumdar D, Xiao G (2005) In situ detection of single micron-sized magnetic beads using magnetic tunnel junction sensors. Appl Phys Lett 86:253,901
154. Shendure J, Mitra RD, Varma C, Church GM (2004) Advanced sequencing technologies: methods and goals. Nat Rev Genet 5:335–344
155. Shendure J, Porreca GJ, Reppas NB, Lin X, McCutcheon JP, Rosenbaum AM, Wang MD, Zhang K, Mitra RD, Church GM (2005) Accurate multiplex polony sequencing of an evolved bacterial genome. Science 309:1728–1732
156. Singh-Gasson S et al (1999) Maskless fabrication of light-directed oligonucleotide microarrays using a digital micromirror array. Nat Biotechnol 17:974–978
157. Smith C (2005) Getting down to details. Nature 435:991–994
158. Song Y, Li Z, Liu Z, Wei G, Wang L, Sun L (2005) Immobilization of DNA on 11-mercaptoundecanoic acid-modified gold (111) surface for atomic force microscopy imaging. Microsc Res Tech 68(2):59–64
159. Sun S, Zeng H (2002) Size-controlled synthesis of magnetite nanoparticles. JACS 124:8204–8205
160. Tanase M, Baurer L, Hultgren A, Silevitch DM, Sun L, Reich DH, Searson PC, Meyer GJ (2001) Magnetic alignment of fluorescent nanowires. Nano Lett 1:155–158
161. Thomson W (1857) On the electro-dynamic qualities of metals. Proc R Soc Lond 8:546–550
162. Togawa K, Sanbonsugi H, Sandhu A, Abe M, Narimatsu H, Nishio K, Handa H (2005) High sensitivity InSb Hall effect biosensor platform for DNA detection and biomolecular recognition using functionalized magnetic nanobeads. Jpn J Appl Phys 44(49):1494–1497
163. Tondra M, Porter M, Lipert RJ (2000) Model for detection of immobilized superparamagnetic nanosphere assay labels using giant magnetoresistive sensors. J Vac Sci Technol A 18(4):1125–1129
164. Tondra M, Granger M, Fuerst R, Porter M, Nordman C, Taylor J, Akou S (2001) Design of integrated microfluidic device for sorting magnetic beads in biological assays. IEEE Trans Magn 37:2621–2623
165. Umek RM et al (2001) Electronic detection of nucleic acids: a versatile platform for molecular diagnostics. J Mol Diagn 3(2):74–84
166. Vaughan RD, O'Sullivan CK, Guilbault GG (1999) Sulfur based self-assembled monolayers (SAM's) on piezoelectric crystals for immunosensor development. Fresen J Anal Chem 364:54–57
167. Vavassori P, Metlushko V, Ilic B, Gobbi M, Donolato M, Cantoni M, Bertacco R (2006) Domain wall displacement in Py square ring for single nanometric magnetic bead detection. Appl Phys Lett 93:203,502
168. Wang SX, Bae SY, Li G, Sun S, White RL, Kemp JT, Webb CD (2005) Towards a magnetic microarray for sensitive diagnostics. J Magn Magn Mater 293:731–736
169. Wojczykowski K, Meißner D, Jutzi P, Ennen I, Hutten A, Fricke M, Volmer D (2006) Reliable stabilization and functionalization of nanoparticles through tridentate thiolate ligands. Chem Commun 21(35):3693–3695
170. Yuasa S, Nagahama T, Fukushima A, Suzuki Y, Ando K (2004) Giant room-temperature magnetoresistance in single-crystal Fe/MgO/Fe magnetic tunnel junctions. Nat Mater 3:868–871
171. Zhao X, Cai Y, Wang T, Shi Y, Jiang G (2008) Preparation of alkanethiolate-functionalized core/shell Fe_3O_4/Au nanoparticles and its interaction with several typical target molecules. Anal Chem 80:9091–9096